

Distribution Agreement

In presenting this thesis as a partial fulfillment of the requirements for a degree from Emory University, I hereby grant to Emory University and its agents the non-exclusive license to archive, make accessible, and display my thesis in whole or in part in all forms of media, now or hereafter now, including display on the World Wide Web. I understand that I may select some access restrictions as part of the online submission of this thesis. I retain all ownership rights to the copyright of the thesis. I also retain the right to use in future works (such as articles or books) all or part of this thesis.

Sunmin Kim

April 13, 2023

Mixed Proportions of Paraloid B-72 and B-48N as Structural Adhesives for Art Conservation:
Evaluations of Tensile Strength and Glass Transition

by

Sunmin Kim

Connie B. Roth
Advisor

Physics

Connie B. Roth
Advisor

Renee A. Stein
Advisor

Eric Weeks
Committee Member

2023

Mixed Proportions of Paraloid B-72 and B-48N as Structural Adhesives for Art Conservation:
Evaluations of Tensile Strength and Glass Transition

By

Sunmin Kim

Connie B. Roth

Advisor

An abstract of
a thesis submitted to the Faculty of Emory College of Arts and Sciences
of Emory University in partial fulfillment
of the requirements of the degree of
Bachelor of Science with Honors

Physics

2023

Abstract

Mixed Proportions of Paraloid B-72 and B-48N as Structural Adhesives for Art Conservation: Evaluations of Tensile Strength and Glass Transition

By Sunmin Kim

This study aims to enhance the understanding of polymer-based adhesive performance in art conservation by focusing on the impact of blending Paraloid B-72 and B-48N polymers to improve resistance to temperature changes and increase strength. In working to restore irreplaceable artifacts, the art conservation field is limited to the use of adhesives that are imperceptible, of appropriate strength, and fully reversible. While conservators have heavily relied on the stable and fully-removable adhesive bonds formed by B-72, its relatively low glass transition temperature T_g leaves adhesive joints susceptible to deformation or failure at hotter temperatures. To address this issue, conservators have incorporated B-48N into blends with B-72 in efforts to raise an adhesive's T_g and resistance to softening at higher temperatures. However, the extent to which the addition of B-48N affects the performance of an adhesive in terms of its strength and resistance to climate fluctuations remains ill-understood. We fill this gap using ellipsometry to measure the glass transitions of various B-72 and B-48N blends. Further, we evaluate each adhesive's tensile fracture strength using the Conservation Adhesive Tensile-to-Shear (CATS) tester. The results provide comprehensive profiles of adhesive properties for conservators to refer to when determining a treatment most suitable for an artifact's expected stresses and location of display. Furthermore, the findings contribute to a deeper understanding of the physics underlying the behavior of polymer blends in the context of art conservation. Most notably, this study finds that tensile fracture strength generally increases with increasing B-48N content with blends with less than 50% B-48N content likely exhibiting similar stability to B-72. While blends with over 50% B-48N concentration exhibit similar strength to neat B-48N, they feature distinct glass transition shapes, broadening the adhesive's glass transition and retaining mechanical properties across a wider temperature range.

Mixed Proportions of Paraloid B-72 and B-48N as Structural Adhesives for Art Conservation:
Evaluations of Tensile Strength and Glass Transition

By

Sunmin Kim

Connie B. Roth

Advisor

A thesis submitted to the Faculty of Emory College of Arts and Sciences
of Emory University in partial fulfillment
of the requirements of the degree of
Bachelor of Sciences with Honors

Physics

2023

Acknowledgements

I would like to express my deepest gratitude to all those who have supported and contributed to the completion of this Honors thesis.

First and foremost, I would like to thank my advisor, Dr. Connie Roth, for her invaluable guidance, encouragement, and expertise throughout this project. Over the past two years where I have had the honor of working in her lab, her support, patience, and mentorship have been instrumental in my growth as a researcher. I am endlessly grateful for the numerous resources, opportunities, and time that Dr. Roth has generously provided me, and it has been an immense pleasure to conduct research in her lab.

I would also like to acknowledge the graduate students in the Roth lab, Jamie Merrill and Alex Couturier, as well as the now Ph.D. holding Dr. Yannic Gagnon and Dr. Louis Han, for their assistance and camaraderie during my time as a student researcher. When I first joined the Roth lab, I struggled to put on safety gloves. These guys have taught me everything I know in experimental work and their friendship has always made the lab a welcoming and enjoyable learning environment.

Special thanks to my Honors committee member and head conservator of Emory's Michael C. Carlos Museum, Renee Stein, for her technical support and sharing of her art conservation knowledge. Renee has provided helpful feedback and advice at various stages of this project and has allowed me the wonderful experience of seeing the applications of my research up close at the Parsons Conservation Lab.

Finally, I would like to thank my family and friends for their unwavering support and encouragement during the completion of this thesis. Their love and belief in my success has been a constant source of strength and motivation.

Table of Contents

Chapter 1: Introduction	1
1.1 Motivation	1
1.1.1 Art Conservation	1
1.1.2 Polymer Physics' Insight into Art Conservation	2
1.1.3 Paraloid B-72 and B-48N as Conservation Adhesives	4
1.2 Goals of Thesis	6
Chapter 2: Introduction to Polymer Physics	8
2.1 The Glass Transition	8
2.1.1 The Glass Transition Temperature (T_g) and Thermal Expansion (α)	8
2.1.2 Tensile Fracture Strength	12
2.2 Polymers in this Study	14
Chapter 3: Experimental Methods–Ellipsometry	18
3.1 Ellipsometry Theory	18
3.1.1 Instrumentation and General Overview	19
3.1.2 Characterizing the Polarization State of Light	19
3.1.3 Interaction Between Light and Matter	22
3.1.4 Fundamental Equation of Ellipsometry	24

3.2	Sample Preparation	26
3.3	Experimental Procedure	28
Chapter 4: Experimental Methods –Conservation Adhesive Tensile-to-Shear (CATS)		
	Tester	30
4.1	Design of CATS Apparatus	30
4.2	Sample Preparation	32
4.2.1	Adhesive Preparation	32
4.2.2	Glass Rod Sample Preparation	33
4.3	Experimental Procedure	35
4.3.1	Measurement Procedure: Improvements over Previous Method	35
4.3.2	Preliminary Testing and Comparison with Previous Results	37
Chapter 5: Results and Discussion		
	39	
5.1	Evaluations of Tensile Strength: Results of CATS Testing	39
5.1.1	Reproducibility of B-72 and B-48N Tensile Strength	39
5.1.2	Tensile Strength of B-72:B-48N Blends	40
5.2	Evaluations of Glass Transition: Results from Ellipsometry	42
5.2.1	A-11 Control: PMMA	42
5.2.2	Pure B-72 and B-48N	45
5.2.3	Blends of B-72 and B-48N	47
5.3	Relating Glass Transition to Adhesive Fracture Strength	53
Chapter 6: Conclusions		
	54	
6.1	Summary of Results	54

6.2 Future Work 55

References 58

List of Tables

2.1	Table of polymers studied in this thesis and their material properties.	16
3.1	Table of polymer solutions used to spin-coat samples.	26
5.1	Table of average tensile fracture strength measured for all samples.	41
5.2	Table of measured T_g values for all samples.	48

List of Figures

1.1	Types of adhesive failure.	3
2.1	Illustration of a polymer and monomer.	8
2.2	Diagrams depicting changes in a polymer's volume and thermal expansion at the glass transition.	9
2.3	Diagram depicting changes in the T_g of a B-72 solution throughout solvent evaporation.	10
2.4	Diagrams depicting changes in a polymer's density and refractive index at the glass transition.	11
2.5	Log modulus of a polymer versus temperature.	13
2.6	Tensile, shear, and compression forces acting on sculptural repairs.	13
2.7	Monomers making up A-11, B-72, and B-48N.	15
3.1	Schematic diagram of the ellipsometer.	18
3.2	Depiction of light as an electromagnetic wave.	20
3.3	Diagram depicting components of \vec{E} along the directions parallel and perpendicular to the surface plane of incidence.	21
3.4	Classifications of light polarization.	22
3.5	Optical layer model used to explain ellipsometry theory.	23
3.6	Ellipsometry layer model.	27
3.7	Photograph of the J.A. Woollam M-2000 spectroscopic ellipsometer.	28

4.1	3D renderings of the CATS Tester (a) in its entirety and (b) zoomed into the sample chamber.	31
4.2	Photograph of the CATS Tester.	33
4.3	Photograph of drying rack used for adhered glass rod sample preparation.	34
4.4	Forces acting on a glass rod sample during CATS testing.	36
4.5	Results of preliminary CATS testing.	37
5.1	Results of B-72 and B-48N tensile fracture strength measurements.	40
5.2	Average tensile fracture strength versus percentage B-48N in the polymer blend. . .	41
5.3	Sample geometry of a polymer thin film.	42
5.4	Normalized film thicknesses of two A-11 samples.	43
5.5	Thermal expansivity of A-11 against temperature.	45
5.6	Normalized film thickness and thermal expansivity of B-72 against temperature. . .	46
5.7	Normalized film thickness and thermal expansivity of B-48N against temperature. .	47
5.8	Normalized film thickness and thermal expansivity against temperature for all polymer blends studied in this thesis.	50
5.9	Comparison of thermal expansivity versus temperature for all polymer blends. . . .	51
5.10	Normalized film thickness and thermal expansivity of 1-1 B-72:B-48N against temperature.	52

CHAPTER 1

INTRODUCTION

1.1 Motivation

1.1.1 Art Conservation

In the field of art conservation, materials of cultural and historical significance are stabilized and restored under the guiding principle that their original states have intrinsic value worth preserving for the long-term future. At times conservation treatments will require the use of adhesives to restore and maintain an artifact's structural integrity and original aesthetic appearance. Because the field champions the concept that "an original state is superior to a changed one," conservators must carefully consider the physical properties of a proposed adhesive prior to incorporating it into a valued object and risking irreversible alteration.¹

Of the many properties that a conservator seeks in an adhesive treatment, the most notable include imperceptibility, long-term stability, appropriate strength, and complete reversibility.^{1,2} The last property listed, reversibility, refers to the ability of an adhesive to be removed without causing any physical or chemical harm to the adhered substrate and is one of the first properties that conservators must consider in a proposed treatment.¹⁻⁴

With the expectation that a conservation treatment need not be repeated for at least 20 years at a minimum, an adhesive bond must remain chemically stable, imperceptible, and able to be completely removed should reassembly or discovery of a more suitable treatment occur throughout the duration of its application.¹ Further, an adhesive must be of appropriate strength in order to support the load of a conserved object without causing it any stresses leading to new fractures.¹

Each conservation project is unique, involving different substrate materials and working environments. As such, no single adhesive exists as a universal solution meeting all the desired criteria under all conditions. Therefore, it is imperative that the physical and empirical proper-

ties characterizing the component materials of adhesives be measured for a variety of different treatments. In investigating these materials, we seek to illuminate the conservator's choice of an adhesive most appropriate and suitable for a project.

1.1.2 Polymer Physics' Insight into Art Conservation

Although natural animal-, starch-, and cellulose-based adhesives have historically been used in the field, modern conservation typically employs the use of synthetic thermoplastic acrylic polymers, which may be easily manipulated by undergoing their glass transition.^{1,2}

By dissolving acrylic polymer resin into a volatile solvent, conservators can create an adhesive that takes advantage of the polymer's glass transition upon solvent evaporation, wherein the polymer transitions from a liquid rubber to a solid glass. With high enough solvent content, a polymer may remain in its equilibrium liquid state at room temperature and have low enough viscosity to be evenly applied to an object under repair using a paint brush. Given sufficient drying time for solvent evaporation, the polymer in the adhesive undergoes its glass transition and settles into a solid bond. Because the adhesive bond is cured through the glass transition, re-applying solvent to the join returns the adhesive to its equilibrium liquid state. Thus, thermoplastic acrylic polymer-based adhesives are fully reversible and suitable for use in art conservation.¹⁻⁷

The glass transition temperature (T_g) of the underlying polymer in a structural adhesive, or the temperature at which that polymer transitions from its liquid to solid state on cooling, is a strong determinant of a cured adhesive bond's flexibility and strength at room temperature.¹ For instance, stiffer, more rigid polymers are typically correlated with a higher T_g and generally form stronger adhesive bonds that are more resistant to deformation under stress. In contrast, adhesive bonds formed out of polymers with a lower T_g generally demonstrate lower adhesive strength but a greater flexibility that may be more suitable for accommodating irregular surfaces with non-uniform stress distribution.¹

Because conserved objects are typically intended to be displayed or studied at room temperature, the art conservation field prefers to utilize polymers with a T_g slightly higher than around

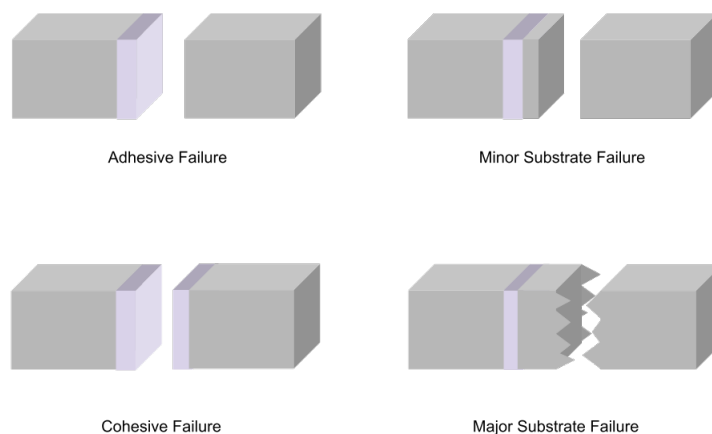


Figure 1.1: Different ways in which failure may occur in an adhesive treatment. The adhesive bond applied to the conserved object is colored in purple. Adhesive and cohesive failure on the left occur due to the adhesive being too weak. Substrate failures on the right occur due to the adhesive being too strong.

25 °C.^{1,8} By incorporating a polymer with a T_g slightly higher than room temperature, conservators can ensure that resulting adhesive bonds are fully solid in a museum or laboratory setting once sufficient solvent evaporation has occurred. In contrast, adhesive bonds formed by a polymer with a T_g significantly higher than 25 °C undergo the glass transition and solidify well above room temperature when there is still a considerable amount of residual solvent left in the join. As a result, air pockets and voids are left in the solid join as residual solvent evaporates over time. Therefore, we can identify how T_g significantly higher than room temperature may predict the formation of a stiff yet brittle bond that may not respond well to movement in a repaired object.^{1,2}

Although examining a polymer's T_g may serve as an informative predictor of bond strength, direct measurements of fracture strength, the maximum stress or force per unit area that a material can support before failure, are necessary to guarantee that an adhesive will support the expected stresses of a repaired object.¹ The fracture strength will be affected by both the plasticizing effects of any remaining solvent in the join, as well as the inherent strength of the polymer itself. If an adhesive is too weak, failure may occur between the adhesive-object interface (adhesive failure) or in the adhesive itself (cohesive failure).³ Therefore, it is crucial that the selected adhesive has

a slightly lesser strength than that of the conserved material in order to ensure that any potential failure will occur in the adhesive or at the bond interface rather than in the artifact itself.¹ Figure 1.1 provides schematics of the different ways an adhesive treatment may fail due to inappropriate strength-matching and further motivates the need to investigate the physical properties of the underlying polymers used in adhesive treatments prior to their incorporation.

1.1.3 Paraloid B-72 and B-48N as Conservation Adhesives

Of the many available synthetic polymers, the acrylic co-polymer Paraloid B-72 by Rohm and Haas has been most frequently used because it has been well-established to form a reliably stable, reversible, and appropriately stiff adhesive for structural repair.^{1-5,7} Since Stephen Koob's 1986 publication⁴ that detailed how to best prepare and apply a 1:1 B-72 and acetone adhesive, as well as further studies that would confirm B-72's strength and reversibility^{3,5-7}, Paraloid B-72 has been popularly used as a conservation treatment.

However, although B-72 has been dubbed the standard of stability for polymer-based adhesives, it is—as are all thermoplastic adhesives—susceptible to ‘creep’ under the influence of elevated temperatures and long-term stress.^{5,6} Creep refers to mechanical deformations such as the slumping or failure of an adhesive over time and is likely to occur when the ambient temperature approaches a polymer's T_g .¹ This is due to the fact that as temperatures near T_g , the segmental motions of the polymer chain gain enough thermal energy to reposition and accommodate the stresses imposed by the conserved object's load.¹

Furthermore, as increased mobility of the polymer chain is associated with an increase in the polymer's volume, adhesive bonds will expand as temperatures rise. Because the thermal expansivity of the polymer differs from that of the conserved material, it is likely that the adhesive will expand differently than the rest of the repair, thereby risking the deformation or failure of the conserved object.² Thus, fluctuating environmental conditions potentially hold devastating effects on the structural integrity of adhesive-repaired objects, particularly when temperatures near a polymer's T_g . Therefore, in addition to the glass transition temperature T_g , conservators must take

notice of a polymer's softening temperature, which marks the onset of the glass transition, in order to understand the full working range of a treatment adhesive.⁶

As B-72 has a relatively low T_g of 40°C, adhesive bonds formed out of B-72 are highly susceptible to creep when they are removed from the climate-controlled museum and subjected to hotter and fluctuating temperatures as in storage, transportation, or outdoor display.^{4,9} In efforts to counteract creep in hotter environments, conservators have begun to incorporate Paraloid B-48N, a polymer with a higher T_g of 50 °C, into mixtures with B-72 as a means to raise an adhesive's T_g .^{10,11} Most notably, adhesive bonds formed from a 3:1 blend of B-72 and B-48N tested by conservator Donna Strahan in the late 1990s demonstrated the sufficient strength, reversibility, and creep resistance required to withstand the extreme climate variations of the Mediterranean.¹⁰ Since then, further studies such as the one conducted by Ting Tan et al. have examined the long-term stability of a 3:1 blend and have discovered both an improved resistance to creep and a longer service life than that of a pure B-72 adhesive.¹² These results have sparked interest in the use of a 3:1 B-72:B-48N adhesive in the field and have resulted in the mixture's use as the primary conservation treatment in large-scale structural projects such as the Metropolitan Museum (Met)'s restoration of Tullio's *Adam*.⁵

A different blend, which incorporated a 1:1 ratio of B-72 and B-48N, was also used for archaeological conservation work in El-Kurru, Sudan, where daytime high temperatures reach up to 45 °C.¹³ This blend was discovered to produce bonds with better stability and long-term reversibility than bonds formed purely out of B-72, which would slump and fail after approximately two years of use in the sub-Saharan desert setting.¹³ Following these reconstruction projects, Jessica Betz investigated the four-point bend flexural strength of neat B-72, neat B-48N, and 3:1 and 1:3 mixture-based adhesives to discover that while the weight at failure was similar for each of the adhesives, the adhesives incorporating B-48N demonstrated a longer time to failure when strength testing was conducted under thermal cycling.⁶

While the addition of B-48N to B-72 has been shown in several studies to raise the T_g of an adhesive and reduce susceptibility to creep, it remains largely unknown to what extent B-48N

will control the performance of an adhesive in terms of its tensile fracture strength, breadth of glass transition, and tendency to thermally expand. As expressed above, these properties must be well-understood and documented in order to elucidate which choice of adhesive is most suitable for a given restoration project and its intended environment of display or storage. As such, there lies motivation to perform stress tests on the mixtures of B-72 and B-48N and to analyze how the properties of these adhesives change with respect to changing temperatures.

1.2 Goals of Thesis

By probing the physical properties of a treatment material prior to its incorporation into a valued artifact, conservators can understand how a material will perform in terms of its imperceptibility, stability, strength, and reversibility—the principles that determine the viewing experience and long-term survival of a conserved object.³ Although B-72 has been a popular choice of structural adhesive due to its fulfillment of these principles, it has also displayed high susceptibility to creep due to its relatively low T_g .^{1,3,4,6} As creep poses an alarming threat to the structural integrity of a treated object—particularly when that object will be subject to extreme climate fluctuations—conservators have recently introduced the addition of B-48N to B-72 in their projects. Because B-48N is a stiffer polymer with a higher T_g than B-72, it is incorporated into a treatment with the expectation that it will raise an adhesive's T_g and thereby bolster its strength and resistance to changes in ambient temperature.^{5,10,11} Although previous studies have conducted stress-testing and investigations into the T_g and creep resistance of 3:1 B-72:B-48N, it remains ill-understood the extent to which the addition of B-48N to an adhesive solution will alter the cured adhesive bond's strength, glass transition, and thermal expansivity.

In this thesis, we seek to determine how varying the proportion of B-48N blended with B-72 will affect the tensile fracture strength of a cured adhesive bond. Thus, the results of this study should provide a complete profile of fracture strength that a conservator may refer to when choosing an adhesive to match the strength of their artifact. Furthermore, we seek to investigate the range of temperatures at which these various polymer blends will experience their glass transition,

as this will enlighten how each adhesive will behave in terms of softening or thermal expansion when ambient temperatures fluctuate around their T_g . In this work, glass rod samples will be adhered with bonds formed of varying B-72 and B-48N ratios and subsequently evaluated for their tensile fracture strength through the use of a device that imposes loads onto a bond until it is broken. We will also prepare thin-film samples for each polymer blend and utilize ellipsometry to measure each mixture's T_g and changes in thermal expansivity over a broad spectrum of temperatures.

CHAPTER 2

INTRODUCTION TO POLYMER PHYSICS

2.1 The Glass Transition

2.1.1 The Glass Transition Temperature (T_g) and Thermal Expansion (α)

A polymer is a large molecular chain composed of repeating chemical units known as monomers.¹⁴ Depending on the amount of thermal energy available, the molecular movements of a polymer are either restricted or free-flowing, leading to differing mechanical properties of a polymer at different temperatures. At high temperatures, the molecules that make up a polymer easily flow past one another and thus flow in response to any stress.¹ At this stage, the polymer is in its equilibrium liquid phase and is referred to as a rubbery melt. However, as a polymer is cooled, cooperative molecular dynamics dramatically slow until the molecular units become ‘frozen-in’ or locked into a random configuration.¹⁴ The polymer system loses ergodicity, or the ability to explore all possible configurations prior to further cooling, and therefore falls out of equilibrium.^{14,15} At this point, the polymer exhibits an extremely high modulus as an amorphous solid and is referred to as a glass.¹⁴ The change from a liquid to a solid on cooling is known as a polymer’s glass transition and the temperature at which this transition occurs is referred to as the glass transition temperature or T_g .¹⁴

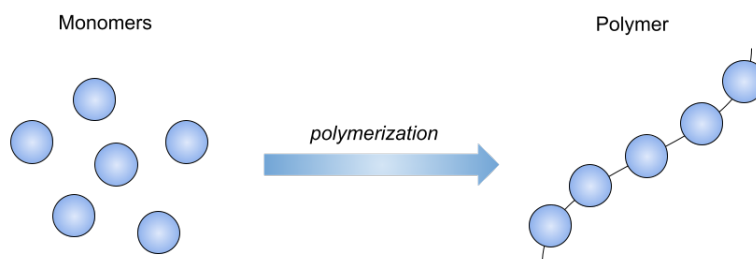


Figure 2.1: Illustration of a collection of monomers, or small molecules, that polymerize to form a long chain of molecular units otherwise known as a polymer.

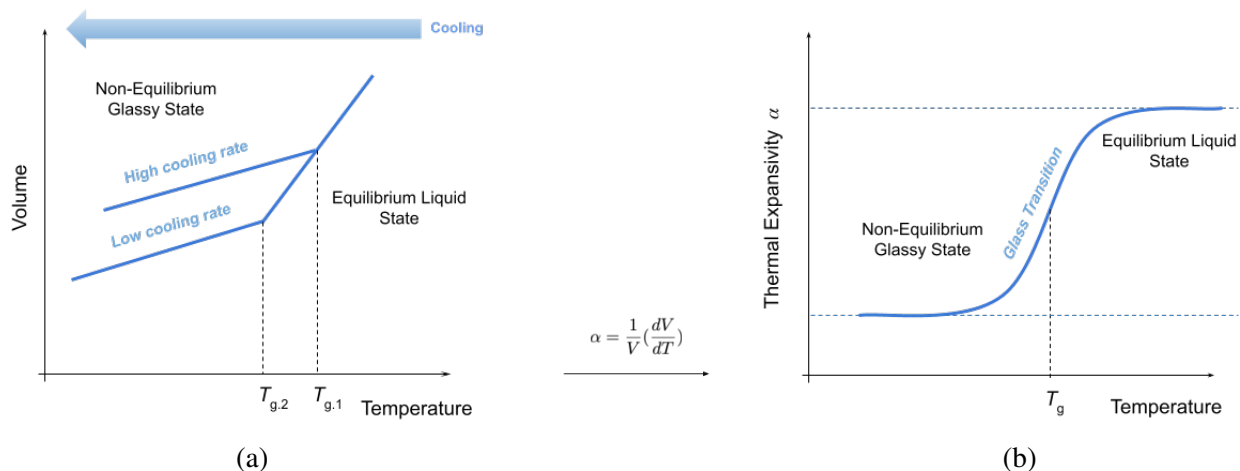


Figure 2.2: Schematic diagrams representing changes in a polymer's (a) volume versus temperature for two different cooling rates and (b) thermal expansivity versus temperature. We identify the glass transition temperature T_g in part (a) as the temperature at which the volume rate of change changes. In (b), thermal expansivity is obtained as the first-order derivative of the polymer's volume with respect to temperature.

The T_g of a polymer may be experimentally determined by recording changes in the polymer's volume on cooling and identifying the temperature at which the polymer's volume rate of change transitions from one slope to another. In a plot of polymer volume versus temperature, T_g is determined as the intersection of the two linear slopes representing the liquid and glassy states of the polymer. It is important to note that the glass transition is a kinetic transition because the measurement of T_g is dependent on the experimental cooling rate, or how quickly the polymer is brought out of equilibrium.¹⁴ As seen in Figure 2.2a, a faster cooling rate results in the formation of a glass with a greater volume than that of one created using a slower cooling rate. This is due to the fact that for a slower cooling rate, a polymer may continue to equilibrate and explore low-energy configurations for a longer time on cooling. In contrast, there is a faster decrease in available thermal energy for a polymer being cooled at a faster rate, which effectively hinders the ability of the polymer's molecular units to cooperatively adjust before being locked into a random configuration at a higher T_g .^{14,15}

A polymer's thermal expansivity may be analyzed by taking the first-order derivative of the polymer's volume dependence on temperature.¹⁴ As shown in Figure 2.2b, a graph of the thermal

expansivity as a function of temperature exhibits two plateaus representing the glassy and rubbery regions of a polymer. While T_g may be measured as the point of inflection in the transition between these two regions, the more insightful observation to extract from this plot is the shape and full range of temperatures over which the glass transition occurs throughout. Through understanding the breadth of glass transition, a conservator may better understand the range of temperatures that the mechanical properties of an adhesive will be particularly sensitive to.

Additionally, the shape of each polymer blend's glass transition and how sharply a polymer blend falls out of equilibrium as a result of changes in temperatures may lend insight into the stability of polymer blends once they have solidified as adhesive bonds at room temperature. For example, a sharp drop in the thermal expansivity curve for a polymer blend's glass transition can indicate that a small deviation from room temperature can lead to a rapid change in adhesive strength. On the other hand, a wider breadth of glass transition can indicate that a polymer blend will be able to maintain its suitable strength and flexibility for a wide range of temperatures and a longer period of time.

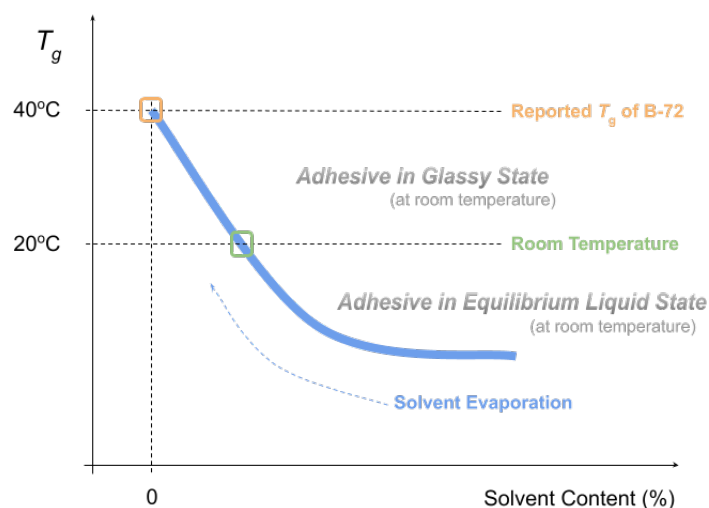


Figure 2.3: Predicted changes in the glass transition temperature T_g of B-72 as solvent content decreases over solvent evaporation. After enough residual solvent has evaporated such that T_g reaches room temperature, the adhesive joint formed by this solution at room temperature transitions from a rubbery melt into a glass.

As conservators typically work with valuable objects sensitive to any dramatic changes in temperature, curing of polymer-based adhesives must be driven by solvent evaporation rather than by direct heating or cooling. When solvent is incorporated into a polymer, it weakens the polymer's inter-molecular bonds and thus promotes greater movement of the polymer's molecular units.² As a result, with a sufficiently high enough solvent content, the T_g of a polymer is effectively lowered such that the polymer may exhibit its rubber-like viscoelastic flow properties at room temperature. As solvent evaporation occurs, T_g is slowly raised and the adhesive bond transitions into a glass once the T_g has increased past room temperature. The process of driving a polymer's glass transition through solvent evaporation is referred to as a solvent quench¹ and is predicted to resemble the plot of T_g versus solvent content in Figure 2.3 based on literature data for how polymer T_g changes with solvent weight fraction.¹⁶ Much like in glass transitions driven by a constant cooling rate, the measurement of T_g when a polymer undergoes its glass transition via solvent-quench likely depends on the solvent evaporation rate, where a faster solvent evaporation rate leads to a higher measurement of T_g and the formation of a higher volume glass than for a polymer undergoing slower solvent evaporation.

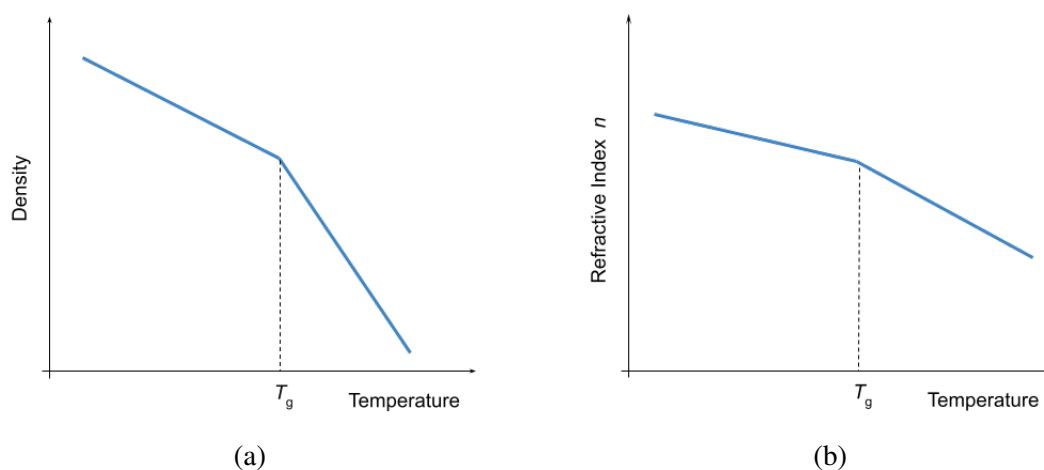


Figure 2.4: Schematic diagrams representing (a) changes in density and (b) refractive index of a polymer against temperature.

In passing from a liquid to a solid, changes in parameters other than volume are also ob-

served in a polymer. The index of refraction n , which quantifies how light interacts with a material, can be monitored through a polymer's glass transition and is an important determinant of how well an adhesive may visually blend in with the conserved adherent.¹ The changes in refractive index are reflected through the changes in a polymer's density with respect to temperature through the Lorentz-Lorentz equation,

$$\frac{n^2 - 1}{n^2 + 2} = \frac{\alpha N_A}{3\epsilon_0 M_0} \rho, \quad (2.1)$$

where we may observe that density ρ is directly proportional to the refractive index via the following constants: Avogadro's number N_A , the permittivity of free space ϵ_0 , and the molecular polarizability α .¹⁷ Figure 2.4 depicts the change in linear slopes that occur on (a) a density versus temperature graph and (b) a refractive index versus temperature graph as a polymer undergoes its glass transition. For both these plots, T_g is measured as the temperature at which the two linear slopes representing the rubbery and glassy states of the polymer intersect.¹⁴

2.1.2 Tensile Fracture Strength

Mechanical properties such as Young's modulus, the ratio comparing the stress resulting from an imposed strain on a polymer, differ depending on whether the polymer exists in its glassy or rubbery state.¹⁵ Figure 2.5 depicts changes in a polymer's modulus as it undergoes the glass transition on cooling.

Art conservators are interested in the stiffness or strength of a polymer's glassy state, as cured polymer-based adhesive bonds are expected to withstand forces acting on artifacts that may be broken at any angle. We may identify some of the different types of forces that may act upon an adhesive system in Figure 2.6.

In Figure 2.6b, we can identify the primary force acting on the adhesive system as a tensile or pulling force. In other words, the forces of gravity and the conserved object's load are exerted perpendicularly to the cross-sectional area of the adhesive bond.³ Meanwhile, the primary force acting on the adhesive system in Figure 2.6a is a shear or sliding force, wherein exerted forces

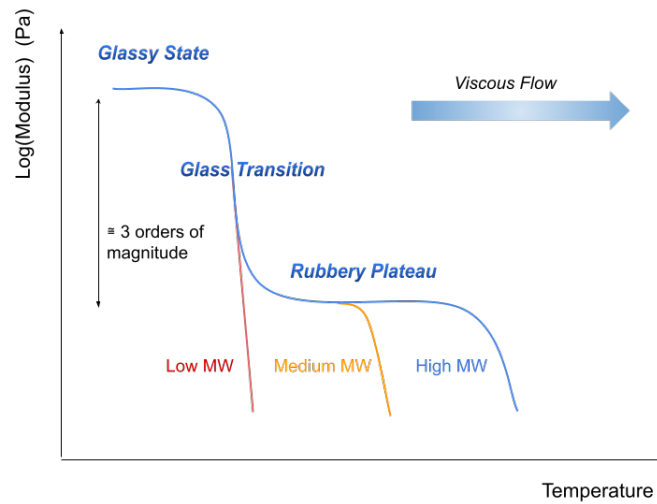


Figure 2.5: Changes in the modulus of a polymer with temperature. The log modulus of a polymer decreases about three orders of magnitude as it undergoes its glass transition. Lower molecular weight (MW) polymers begin to achieve viscous flow at much lower temperatures than do higher MW polymers.

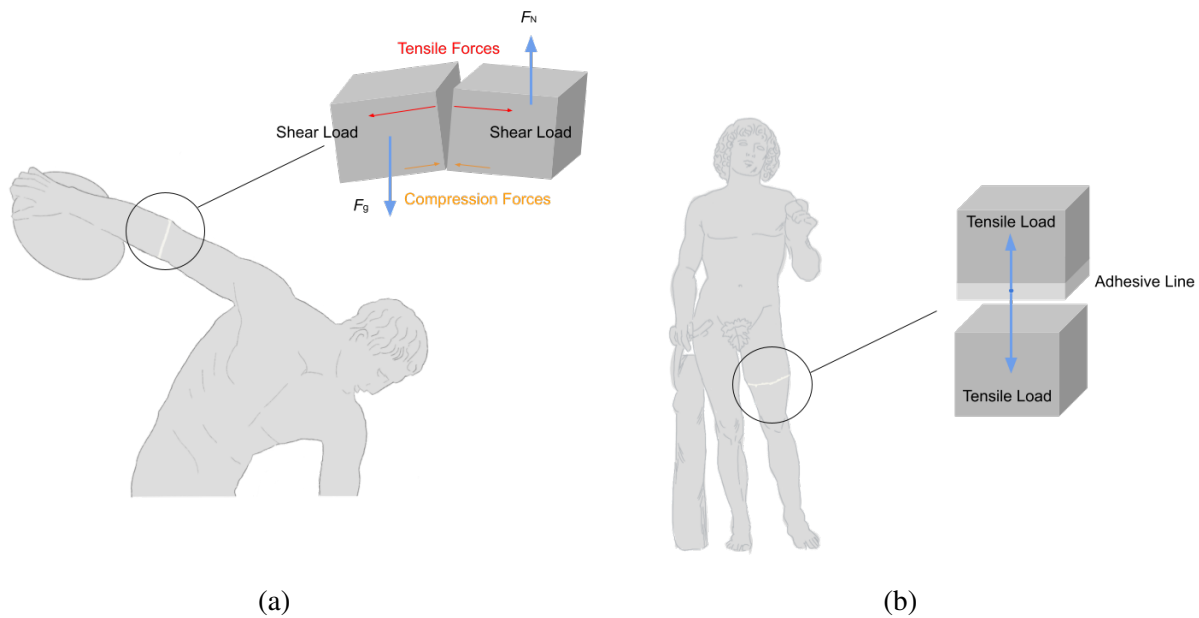


Figure 2.6: (a) Diagram of shear, tensile, and compression forces acting on a structural repair and (b) Diagram of purely tensile forces acting on a structural repair.

are coplanar to the cross-section of the adhesive.³ However, even as the primary force appears to be shear in Figure 2.6a, we may notice that there is actually a combination of shear, tensile, and compression (or pushing) forces acting on the adhesive system. For this reason, this study focuses on evaluating how an adhesive performs under purely tensile forces since these results lend some understanding of how an adhesive may perform under a combination of various different forces.

We may quantify an adhesive's performance under tensile forces by measuring its tensile fracture strength σ , or the maximum tensile force per unit area that a material can withstand before failing. This quantity may be calculated as:

$$\sigma = \frac{F}{A}, \quad (2.2)$$

where F is the magnitude of the tensile force acting on the material and A is the material's cross-sectional area.

2.2 Polymers in this Study

As previously mentioned, polymer chains are composed of smaller chemical sub-units known as monomers. It is worthwhile to investigate the constituent monomers and molecular structures of each polymer analyzed in this study, as they offer insight into many of the properties we seek to understand. For instance, knowing the monomer molecular weight, chain length, and side groups of a polymer may lend an understanding of the T_g or viscosity of an adhesive solution since increasing any of these quantities will generally increase the polymer molecules' resistance to flow.¹

A-11, or poly(methyl methacrylate) (PMMA), is a homopolymer composed purely of methyl methacrylate. A-11 is reported by its manufacturers to have a high T_g of 100 °C and clearly illustrates why polymers with a T_g significantly higher than room temperature are not suitable for use as primary adhesive treatments in art conservation.¹ Although the glass transition of A-11 may be driven by a temperature quench to produce a strong glassy material (e.g. as PMMA or 'Plexi-

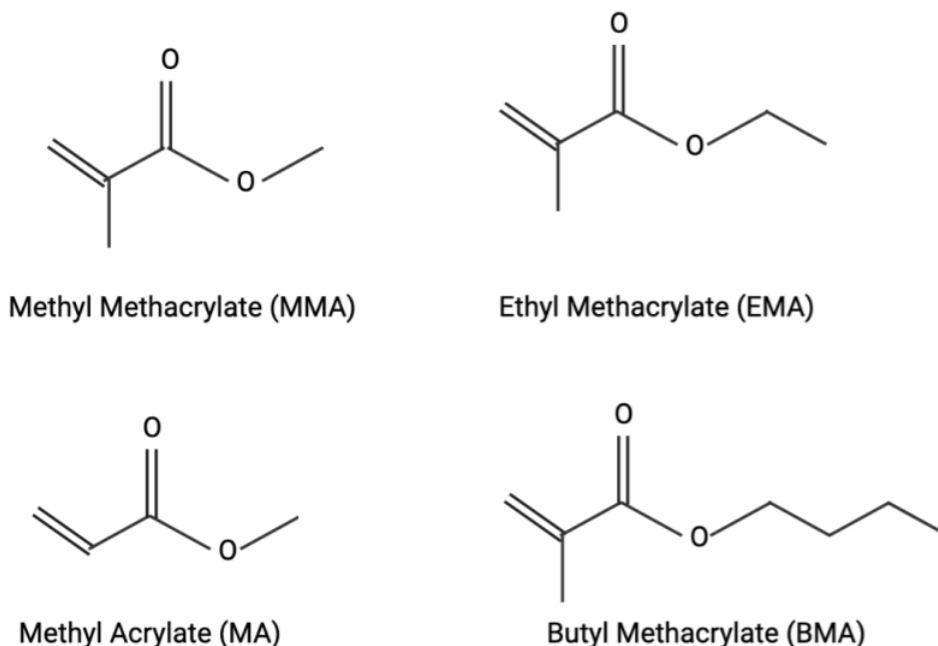


Figure 2.7: Chemical structures of the monomers that predominantly make up A-11, B-72, and B-48N: methyl methacrylate (MMA), ethyl methacrylate (EMA), methyl acrylate (MA), and butyl methacrylate (BMA).

glas' as it is commonly referred to), attempts to prepare an A-11 adhesive bond through a solvent quench, as in art conservation practices, lead to the formation of a brittle bond full of air pockets left by evaporated solvent.⁸ This is because A-11 falls out of equilibrium quicker than the residual solvent is able to evaporate out of the material. For these reasons, conservation treatments rarely incorporate the use of A-11. However, for the purposes of this study, A-11 was selected as a control for the ellipsometry measurements since its behavior has been formerly investigated and is largely understood by our research group.

Paraloid B-72, which is most frequently used by the conservation field, is a random copolymer consisting of 65.8% ethyl methacrylate (EMA), 32 % methyl acrylate (MA), and 2.2% butyl methacrylate (BMA).¹ With a reported T_g of 40°C and refractive index of 1.48, B-72 has long been relied upon in conservation to create appropriately stiff and reversible adhesive bonds.^{1,3,4,6} However, its use in environments with elevated temperatures is questionable due to its relatively low T_g and higher susceptibility to creep compared to other polymers.³

Paraloid B-48N is another acrylic copolymer often used by the art conservation field for coating metals.^{1,10} Composed by 74.5% methyl methacrylate (MMA) and 25.5% butyl methacrylate (BMA), B-48N has a higher reported T_g than B-72 of 50°C.¹ As a result, it has been reported to exhibit greater strength and stiffness at room temperature than B-72.^{10,11} It also results in a solution of slightly higher viscosity, which may be explained by the differences in molecular weight shown in Table 2.1.

Table 2.1: The polymers studied in this thesis. Monomer content, molecular weight (M_w), glass transition temperature (T_g), and refractive index (n) reported at the $\lambda = 589$ nm yellow doublet D-line of sodium as reported by Ref. [1] are provided.

Polymer	Monomer(s)	Molecular Weight, M_w	T_g	Refractive Index, n
A-11	100% methyl methacrylate,	350,000 g/mol	100 °C	1.490
B-72	65.8% ethyl methacrylate, 32% methyl acrylate, 2.2% butyl methacrylate	88,000 g/mol	40 °C	1.479
B-48N	74.5% methyl methacrylate, 25.5% butyl methacrylate	184,000 g/mol	50 °C	1.481

For the purposes of this thesis, we investigate the properties of B-72:B-48N mixtures. Most famously, a 3:1 B-72:B-48N blend was introduced by conservator Strahan as a reliable and creep-resistant adhesive and was subsequently used as the primary adhesive treatment in the Met's restoration of Tullio's *Adam*.^{5,10} In an effort to understand how varying ratios of each respective polymer will affect the behavior of the mixed adhesive, this study investigates solutions of 1:0, 7:1 3:1, 1:1, 1:3, 1:7, and 0:1 B-72:B-48N blends. While these polymer blends have yet to be extensively studied in the field, we may make predictions for each blend's T_g using the Fox equation,

$$\frac{1}{T_g} = \frac{w_1}{T_{g,1}} + \frac{w_2}{T_{g,2}}, \quad (2.3)$$

which estimates the T_g of a polymer blend using w_1 and w_2 , the weight fractions of the two polymers being blended together along with their respective glass transition temperatures $T_{g,1}$ and $T_{g,2}$.¹⁸ A table comparing the literature-reported or predicted T_g of each polymer blend with the experimental values measured in this thesis will be provided in Table 5.2 in the Results and Dis-

cussion chapter.

CHAPTER 3

EXPERIMENTAL METHODS–ELLIPSOMETRY

3.1 Ellipsometry Theory

In order to track and measure important property changes of a polymer across its glass transition on cooling, we make use of an optical instrument known as an ellipsometer. In ellipsometry, we observe changes in the polarization of elliptically polarized light upon its reflection off a polymer thin film sample. Changes in the light's polarization state due to interaction with the polymer are recorded and represented by the ellipsometric angles Psi (Ψ) and Delta (Δ). These principal angles, which respectively characterize the shifts in amplitude and phase difference of the light's orthogonal electric-field components, are used in conjunction with an optical layer model to extract the film thickness $h(T)$ and refractive index $n(T)$ of the polymer as it undergoes the glass transition.

This chapter provides a conceptual tour behind the practices of ellipsometry and details the experimental techniques used to measure the glass transitions of varying B-72:B-48N blends prepared as thin film samples.

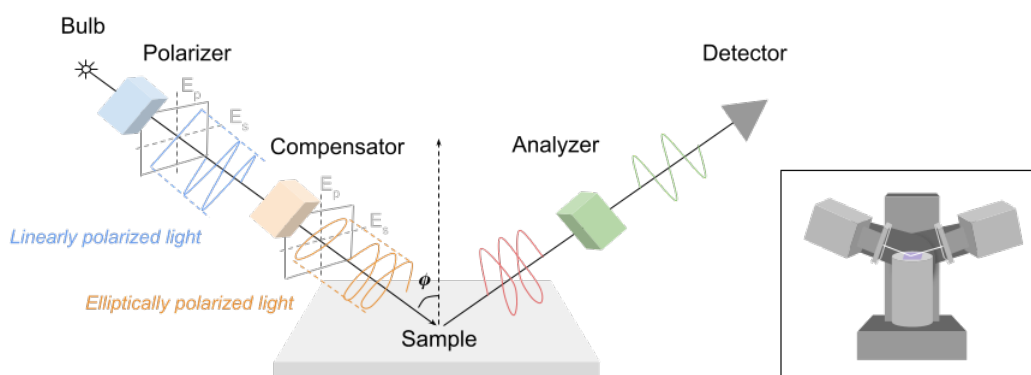


Figure 3.1: A schematic diagram depicting the trajectory of light in an ellipsometer. As the light is shown passing through each component of the instrument, the electric-field intensity vectors corresponding to its current state of polarization are drawn.

3.1.1 Instrumentation and General Overview

We can observe the general set-up of the ellipsometer, as well as the schematic pathway of light followed in an ellipsometric measurement, in Figure 3.1. To obtain a measurement of Ψ and Δ , the ellipsometric angles used to extract the film thickness and refractive index of a polymer sample, unpolarized visible light is first produced from the bulb of the ellipsometer. This light passes through the polarizer, which linearly polarizes the light. The linearly polarized light then travels through the compensator, in which a phase difference $\delta = \frac{\pi}{2}$ between the light's orthogonal electric-field components is introduced, thereby *elliptically* polarizing the light. For the Woollam M-2000 spectroscopic ellipsometer that we utilize in this thesis, the compensator used to elliptically polarize the light is a quarter-wave plate, rotating at 20 rev/s.

Following elliptical polarization, the light travels to the sample stage at the configured angle of incidence ϕ , where it interacts with the polymer film. In traveling through and reflecting off the polymer sample, the light is altered and its state of elliptical polarization as it reaches the analyzer differs from that of the light incident on the polymer. The analyzer reverts the light back to a state of linear polarization and its intensity as a function of wavelength λ is measured by the charge-coupled device (CCD) detector. The ellipsometer software then uses the experimentally-gathered light intensity values to derive Ψ and Δ .

Thus far, we have summarized the trajectory of light in an ellipsometer and have explained how each component of the instrument plays a role in attaining a measurement of Ψ and Δ . The following subsections provide a definition of light polarization and discuss the nature of light as it travels through different media. Further provided are the derivations of Ψ and Δ from basic optical principles as well as the details on how to extract film thickness and refractive index from these parameters through the fundamental equation of ellipsometry.

3.1.2 Characterizing the Polarization State of Light

In electromagnetic theory, light may be described as a transverse electromagnetic wave composed of the time-varying electric- and magnetic-fields \vec{E} and \vec{B} . These fields are mutually

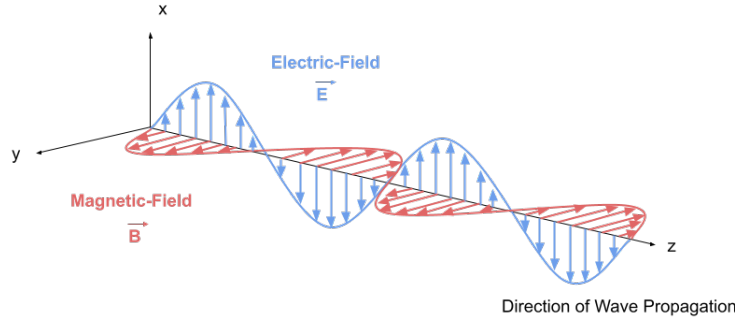


Figure 3.2: Light as an electromagnetic wave. The electric- and magnetic-field components making up the light are mutually orthogonal to one another and to the direction of wave propagation.

orthogonal to one another and to the direction of wave propagation, as shown in Figure 3.2.

In ellipsometry, we are particularly interested in the behavior of the light's electric-field \vec{E} , or rather its state of polarization, as it travels through and interacts with our polymer sample. The space and time-evolution of \vec{E} may be represented by a solution to Maxwell's wave equations, or

$$\vec{E}(z, t) = E_0 \sin\left(\frac{2\pi}{\lambda}(z - vt) + \xi\right),$$

where E_0 represents the amplitude of the electric-field, λ and v denote the wavelength and velocity, and ξ denotes the phase of the wave.¹⁹

We may further decompose this field into two orthogonal components, \vec{E}_p and \vec{E}_s , by defining a plane of incidence. Figure 3.3 depicts light with the electric-field vector \vec{E} shining incident on a sample polymer film. If we define the plane of incidence to contain the sample's surface normal, we may identify \vec{E}_p and \vec{E}_s as the components of \vec{E} that lie parallel and perpendicular to the plane of incidence, respectively.²⁰ The space- and time-evolutions of \vec{E}_p and \vec{E}_s may then be represented by the equations:

$$E_p(z, t) = E_{0,p} \sin\left(\frac{2\pi}{\lambda}(z - vt) + \xi_p\right) \quad (3.1)$$

and

$$E_s(z, t) = E_{0,s} \sin\left(\frac{2\pi}{\lambda}(z - vt) + \xi_s\right). \quad (3.2)$$

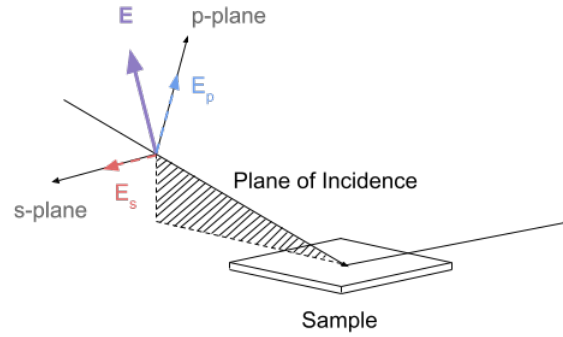


Figure 3.3: Diagram depicting the plane of incidence for light traveling with the electric-field vector \vec{E} . \vec{E} is broken up into two orthogonal components \vec{E}_p and \vec{E}_s , lying parallel and perpendicular to the plane of incidence respectively.

Thus, we can characterize the polarization state of light by observing the phase difference, δ , between the respective phases of the electric-field vectors \vec{E}_p and \vec{E}_s .²⁰

$$\delta = \xi_s - \xi_p. \quad (3.3)$$

For the randomly polarized light that we are used to observing in everyday life, δ varies unpredictably and the electric-field vector \vec{E} is randomly oriented throughout space.²⁰ However, if the two electric-field components combine in-phase such that δ is constant and equal to 0, we describe that light as being linearly polarized.²⁰ Then when observing that light wave in the plane perpendicular to its direction of travel, we observe that its \vec{E} vector traces a line. Otherwise, light with a phase difference of $\delta \neq 0$ is referred to as elliptically polarized (with $\delta = \pi/2$ and $|E_p| = |E_s|$ understood as a special case of circular polarization), and we may observe that the electric-field vector \vec{E} for such light traces out an ellipse.²⁰ The precessions of \vec{E} for randomly polarized, linearly polarized, and elliptically polarized light waves are depicted in Figure 3.4.

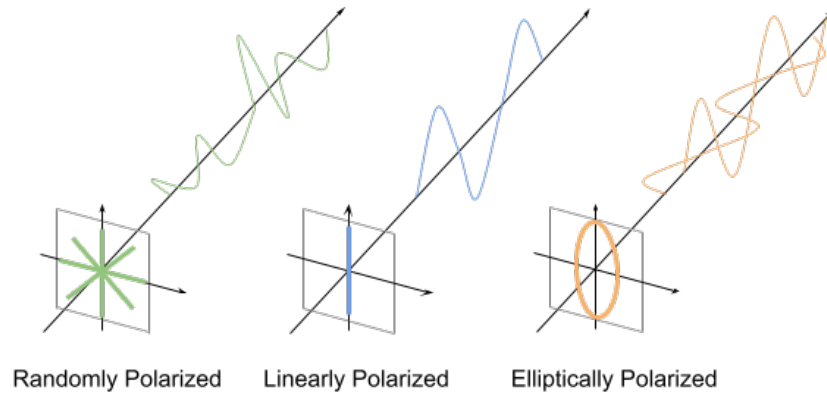


Figure 3.4: The classifications of polarized light. In the plane perpendicular to the direction of wave propagation, we observe the electric-field intensity vector precess along either a linear or elliptical trajectory, depending on the relative phase difference between its orthogonal components. In contrast, the electric-field intensity vector for the randomly-polarized light is randomly-oriented throughout space.

3.1.3 Interaction Between Light and Matter

We proceed by discussing the nature of light as it travels through bulk matter such as our polymer thin film sample. The velocity of light in a given medium is characterized by the index of refraction, which relates such velocity to the speed of light in a vacuum, c , using the equation $n = c/v$.¹⁹ The refractive index differs for different wavelengths λ and for transparent materials such as our polymer thin film samples, can be described by the Cauchy equation,

$$n(\lambda) = A + \frac{B}{\lambda^2} + \frac{C}{\lambda^4}, \quad (3.4)$$

which expands $n(\lambda)$ in powers of $(1/\lambda^2)$ using the optical constants A , B , and C .¹⁷

When light meets the interface between media of different refractive indices, some of the light is transmitted while some is reflected. If light is to meet the boundary between mediums 1 and 2, the law of reflection,

$$\phi_i = \phi_r,$$

tells us that the component of light that reflects from the interface back to medium 1 does so at the

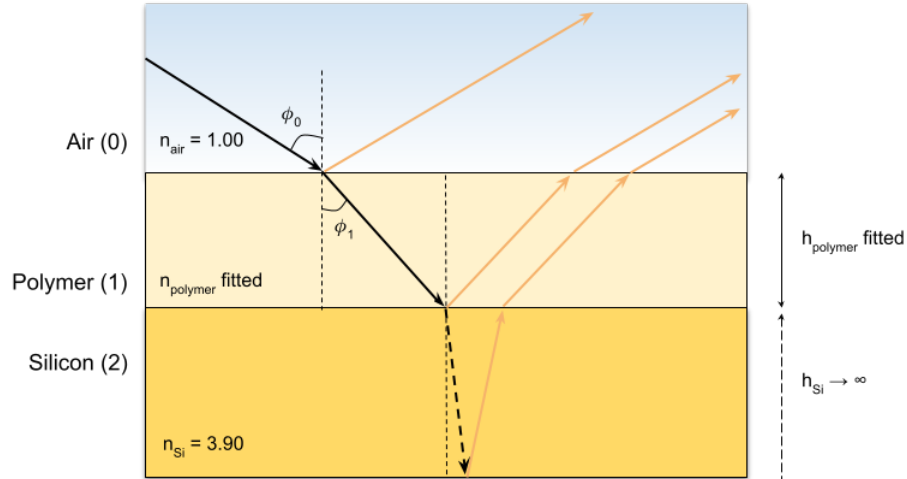


Figure 3.5: Optical layer model used to explain ellipsometry theory. The angles of incidence and refraction are drawn from the surface normal for mediums 0 and 1 as the light travels from the air to the polymer. The reported refractive indices for each medium are provided. The silicon layer is treated as semi-infinite thick.

same angle as the angle of incidence.¹⁹ Meanwhile, Snell’s Law describes the angle at which the component of transmitted light travels through medium 2 using each medium’s refractive index:¹⁹

$$n_1 \sin \phi_1 = n_2 \sin \phi_2. \quad (3.5)$$

We may refer to Figure 3.5 as the sample geometry used to explain the mathematics involved in ellipsometry theory, where a layer of polymer solution rests atop a “semi-infinite” silicon substrate. We observe that as the light enters the polymer from the air at an incident angle ϕ_0 , it follows Snell’s Law to refract at an angle ϕ_1 . Then we may notice that this component of transmitted light encounters the silicon layer with ϕ_1 as the new angle of incidence.

We may characterize the amount of light reflection that occurs at each media interface using the Fresnel reflection coefficients, which compare the electric-field intensity of the light in each medium. For the reflection that occurs as light in our ellipsometric measurement travels from the air (0) to the polymer (1), we may define the Fresnel reflection coefficient r_{01} as²⁰

$$E_{\text{reflected}} = r_{01} E_{\text{incident}}. \quad (3.6)$$

As we have shown that the electric-field of light \vec{E} can be broken into \vec{E}_p and \vec{E}_s components, the Fresnel reflection coefficients for the p - and s -components are defined by

$$r_{01}^p = \frac{n_1(\lambda)\cos(\phi_0) - n_0(\lambda)\cos(\phi_1)}{n_1(\lambda)\cos(\phi_0) + n_0(\lambda)\cos(\phi_1)}, \quad (3.7)$$

and

$$r_{01}^s = \frac{n_0(\lambda)\cos(\phi_0) - n_1(\lambda)\cos(\phi_1)}{n_0(\lambda)\cos(\phi_0) + n_1(\lambda)\cos(\phi_1)}, \quad (3.8)$$

using the angles of incidence and refraction ϕ_0 and ϕ_1 and the wavelength-dependent refractive indices of each medium.²⁰ To characterize the total reflection of the light as it interacts with the first three layers in our sample model, we introduce the *total* Fresnel reflection coefficient as²⁰

$$r_{tot} = \frac{r_{01} + r_{12}e^{-i2\beta}}{1 + r_{01}r_{12}e^{-i2\beta}}. \quad (3.9)$$

Here, we have utilized the Fresnel reflection coefficients characterizing the light reflection in the air-polymer and polymer-silicon oxide interfaces, r_{01} and r_{12} respectively, and have introduced the parameter β , defined as the phase thickness or²⁰

$$\beta = \frac{2\pi hn_1}{\lambda}\cos(\phi_1). \quad (3.10)$$

From this expression, we may finally derive the properties of the polymer we wish to investigate in an ellipsometric measurement: the thickness of the polymer layer, h , and the refractive index of the polymer, n_1 .

3.1.4 Fundamental Equation of Ellipsometry

We conclude our discussion of ellipsometry theory by defining the principal ellipsometric angles Ψ and Δ and explaining how the ellipsometry software derives film thickness h and refractive index n from these parameters.

When elliptically polarized light reflects off a polymer thin film sample during an ellipsometric measurement, the state of elliptical polarization in the reflected light is altered due to interaction with the polymer. We may first denote the change in phase difference δ between the \vec{E}_s and \vec{E}_p components of the incoming and outgoing light using the angle Δ , defined as²⁰

$$\Delta = \delta_f - \delta_i, \quad (3.11)$$

where δ_f and δ_i denote the phase differences of the final and initial light. Furthermore, we may define the angle Ψ to characterize the amplitude of the outgoing elliptically polarized light's electric field \vec{E} by relating the p - and s -components of the total Fresnel reflection coefficients such as²⁰

$$\tan(\Psi) = \frac{|r_{tot}^p|}{|r_{tot}^s|}. \quad (3.12)$$

Ψ and Δ are experimentally determined by an ellipsometric measurement and are related to the film thickness and refractive index of the polymer under inspection by the fundamental equation of ellipsometry,²⁰

$$\rho = \tan(\Psi)e^{i\Delta} = \frac{r_{tot}^p}{r_{tot}^s}. \quad (3.13)$$

This equation relates the complex quantity ρ to the total Fresnel reflection coefficients, which contain information on the polymer's film thickness and refractive index, as seen in Equations 3.9 and 3.10. Because the ellipsometer measures the intensity of elliptically polarized light, I^p and I^s , which relate to ρ as

$$\frac{I^p}{I^s} = \frac{|E^p|^2}{|E^s|^2} = \frac{|r_{tot}^p|^2}{|r_{tot}^s|^2} = |\rho|^2. \quad (3.14)$$

we may compare ρ determined by the experimentally gathered ψ and Δ with a predicted ρ calculated from the Fresnel equations.

For each measurement of Ψ and Δ , the ellipsometry software calculates predicted ρ re-

sponses for the light using the optical layer model shown in Figure 3.5 and the Cauchy model (Eq. 3.4) and compares those values with the experimentally gathered Ψ and Δ values. Through minimizing the mean squared error (MSE) between the predicted and experimental $\Psi(\lambda)$ and $\Delta(\lambda)$ curves, the parameters A , B , and C , as well as the film thickness h , are appropriately fit for our model such that we may finally extract the refractive index and film thickness of the polymer.¹⁷

3.2 Sample Preparation

In this thesis, eight different polymer solutions were prepared as thin film samples and measured with the ellipsometer for their glass transitions on cooling. All of the polymers were produced by Rohm and Haas, a subsidiary of the Dow Chemical Company, and were provided by the Parsons Conservation Lab of Emory University's Michael C. Carlos Museum.

Table 3.1 lists all of these sample polymers, their reported or calculated glass transition temperatures, and the solvents used to dissolve them for thin film sample preparation. The methods of sample preparation and data collection discussed here and in the following section follow the procedure streamlined in Benjamin Kasavan's Honors Thesis.⁹

Table 3.1: The polymer solutions used to prepare thin film samples for ellipsometry in this thesis.

Polymer(s)	Percentage B-48N in Blend (%)	Solvent Used
A-11	0	toluene
B-72	0	toluene
7:1 B-72:B-48N	12.5	8:1 toluene:acetone
3:1 B-72:B-48N	25	
1:1 B-72:B-48N	50	
1:3 B-72:B-48N	75	
1:7 B-72:B-48N	87.5	
B-48N	100	

To create a thin film sample for ellipsometry, acrylic pellets of the polymer (or mixture of polymers) under investigation were first dissolved in the solvent of choice at a 10 weight-percent (wt%) concentration. In the field, art conservators typically utilize acetone as the primary solvent in polymer-based adhesive solutions due to its low toxicity and quick evaporation rate that allows

for faster bond curing. Faster bond curing allows for less solvent absorption to occur in porous substrates and therefore reduces the plasticizing effects of residual solvent that may weaken the adhesive strength of the bond. However, the low boiling point and high volatility of acetone lead to the production of non-uniform film samples in ellipsometry.⁹ This proves troubling for data collection since surface roughness in samples causes light scattering that may dramatically reduce the intensity of reflected light measured by the ellipsometer.²¹ As such, the A-11 and neat B-72 solutions were created using toluene. For any polymer solutions incorporating B-48N, which is not fully soluble in toluene,¹ the choice of solvent was an 8:1 mixture of toluene and acetone discovered in Kasavan's thesis to create smooth film samples.⁹

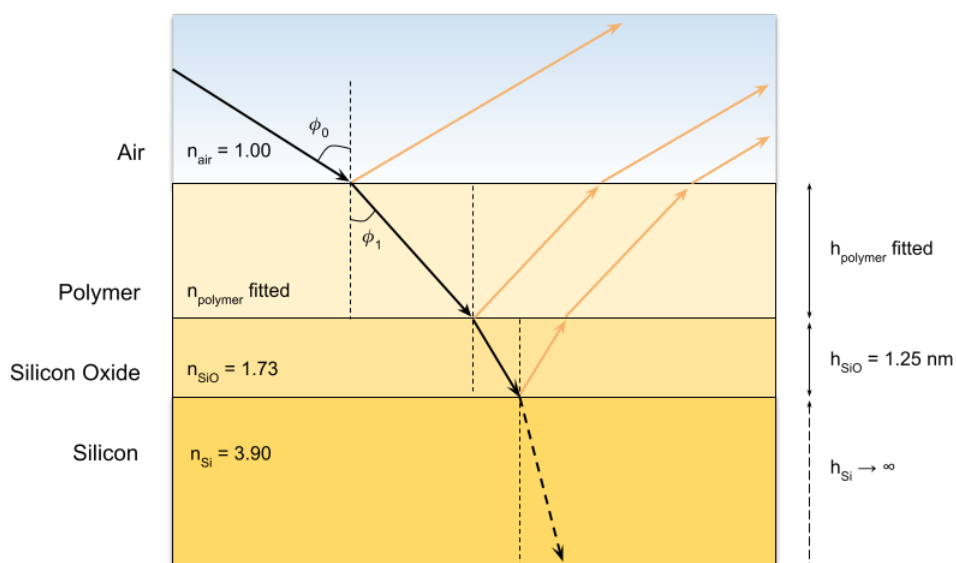


Figure 3.6: Model of the different media interfaces that light travels through in an ellipsometric measurement. The thickness of the silicon oxide layer is set at 1.25 nm and the silicon layer is treated as semi-infinitely thick.

Magnetic stir bars were placed in the solution vials and used to stir the solutions overnight. Polymer films with thicknesses of 700 – 1000 nm were then formed by spin-coating the solutions at 1000 – 3000 rpm onto 2 cm x 2 cm silicon wafers, each with a 1.25 nm thick silicon oxide layer. This step produced the layer model we use, shown in Figure 3.6.

All films were subsequently annealed under vacuum at 90 °C for 18 to 22 hours. Doing so

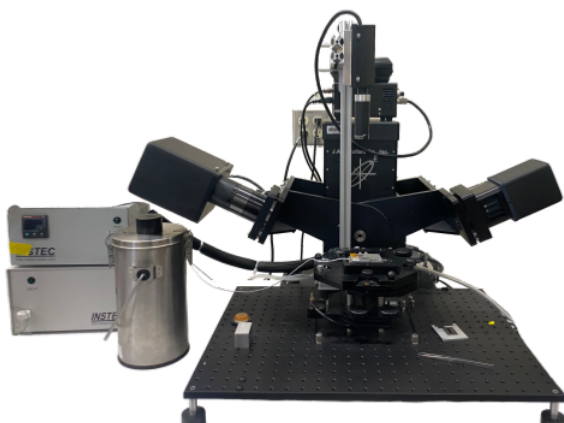


Figure 3.7: Photograph of the J.A. Woollam M-2000 spectroscopic ellipsometer used in this thesis. Attached to the ellipsometer is the HSC 302 heater and a container holding liquid nitrogen.

evaporated residual solvent from the sample films and further allowed for the polymer chains to relax, thereby ensuring uniform thermal histories for all samples prior to their inspection under the ellipsometer. It is important to note that vacuum annealing evaporates all solvent from the polymer thin film sample, such that only the polymer or polymer blend itself is being studied under the ellipsometer.

3.3 Experimental Procedure

Measurements of the glass transition in this thesis were taken using the J.A. Woollam M-2000 spectroscopic ellipsometer equipped with an Instec HSC 302 temperature stage. Two thin film samples of A-11, as well as three thin film samples for each of the remaining 7 different polymer blends under investigation were measured for their thickness h and refractive index n with changes in temperature by observing the following procedure:

Prior to loading sample films onto the ellipsometer, the temperature stage was first brought down to 0 °C before being stabilized at 30 °C. Doing this primed the tubes that deliver liquid nitrogen to the sample stage and therefore allowed for a more constant cooling rate once measurements began.

Once the temperature was preset and the angle of incidence was configured to 65°, annealed

polymer thin film samples were transferred from the vacuum oven and secured to the heating stage of the ellipsometer. Thin film samples were then heated to 150 °C in ten minutes and held at that temperature for twenty minutes. Ellipsometric measurements were then taken for 5 seconds every 10 seconds as the samples were cooled to 0 °C at a cooling rate of 1 °C/min. In an effort to combat water condensation and frost buildup at lower temperatures, dry nitrogen gas was continuously flowed through the sample chamber for the entire duration of measurements at an approximate rate of 1.6 L/min. Ellipsometry measurements of $\Psi(\lambda)$ and $\Delta(\lambda)$ were fit to the optical layer model shown in Figure 3.6 using the Cauchy model (Eq. 3.4) for $\lambda = 400 - 1000$ nm with the native oxide layer held constant at 1.25 nm.

CHAPTER 4

EXPERIMENTAL METHODS – CONSERVATION ADHESIVE TENSILE-TO-SHEAR (CATS) TESTER

In order to evaluate the tensile fracture strengths of adhesive bonds formed by B-72:B-48N blends, we utilize the Conservation Adhesive Tensile-to-Shear (CATS) tester, which was previously designed and constructed by Olivia L.F. Boyd and the Emory Machine Shop for Olivia's Honors thesis.²² The CATS tester was built to stress-test various adhesive bonds by regularly incrementing the amount of weight being applied to a bonded pair of 2-inch, 6 mm diameter borosilicate glass rods. Along with the addition of a manual rotation stage that may be used to vary the angle at which a bond is stress evaluated at, the tester makes it possible to record the maximum weight that bonds can support before failure. Thus, measurements taken from the CATS tester may offer an understanding of an adhesive's performance under the combination of shear and tensile forces. For the purposes of this study, the CATS tester was used to perform purely-tensile stress evaluations in order to measure how increasing proportions of B-48N in B-72 blends would affect tensile fracture strength.

4.1 Design of CATS Apparatus

The base structure of the CATS tester is constructed out of aluminum and consists of a padded base and a backboard held upright by a large support in the back. The portion of the tester where samples are secured is located at the top of the backboard plane. 3D renderings of the entire CATS tester and the top portion where the sample chamber is located are presented in Figure 4.1b. A photographic depiction of the CATS tester is given in Figure 4.2.

The upper sleeve, represented by a blue block in Figure 4.1b, has been drilled to create a 1/2 inch long cavity in which the upper half of the testing sample may be inserted. Once inserted, the sample is secured to the tester by use of the screw in the middle of the block. The upper sleeve

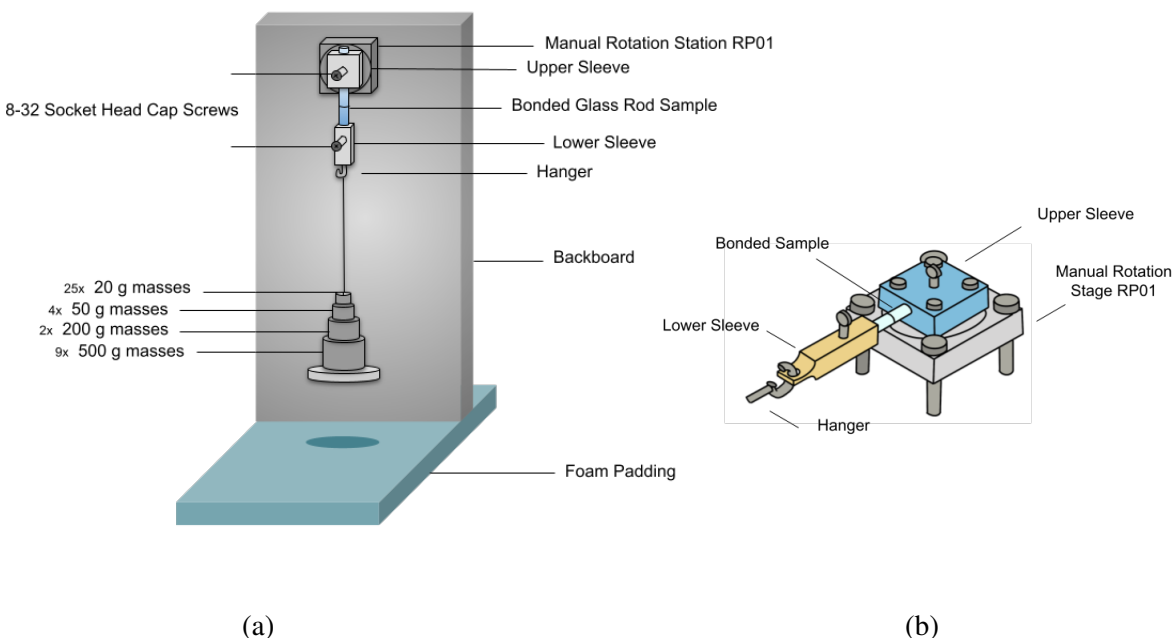


Figure 4.1: 3D renderings of the CATS tester (a) in its entirety and (b) zoomed into the sample chamber. The manual rotation stage on the sample chamber has been colored grey, and the upper and lower sleeves in which glass rod samples are inserted and secured with 8-32 socket head cap screws are colored blue and yellow, respectively. The hanger is attached to the lower sleeve and holds the weights added throughout the experiment.

is screwed on top of the manual rotation stage RP01, which was made by ThorLabs and shown in grey in the figure. With the manual rotation stage, the upper sleeve may be rotated to vary the angle at which the bond is stress-tested.

The yellow rectangular block represents the lower sleeve of the CATS tester. The lower sleeve has also been drilled with a 1 1/2 inch long slot to fit the lower half of the testing sample, which is secured by another screw in the middle of the block. The bottom of the lower sleeve contains a hole into which the hook of the hanger is inserted. The hanger itself is 15 inches long and with the circular 50 g weight screwed to the end of its length, has a total weight of 63 g. Once the bonded glass rod sample has been attached to both the upper and lower sleeves of the CATS tester, slotted weights are added to the hanger at regular intervals until the sample bond is broken. The weight at failure, which is the sum of the hanger weight, added weights, and weight of the adhered glass rod's lower half at the time of failure, may then be converted to give the tensile

fracture strength of the adhesive.

The CATS tester was originally designed to measure how the tensile fracture strength of a B-72 adhesive cast from acetone would change with varying loading levels of fumed silica (FS). As such, components of the CATS tester, such as the hanger length, were designed with consideration of the lower and upper limits of B-72's expected tensile strength. (Details of preliminary testing used to justify all of the design specifications of the CATS tester can be found in Olivia L.F. Boyd's Honors Thesis.²²) However, because this study would evaluate the tensile fracture strengths for a variety of different adhesives, including those with strengths much greater than that of pure B-72, adjustments to the CATS tester's design and measurement protocol were necessary.

In measuring the strengths of B-72 and B-48N blends, the weight being applied to a sample bond often exceeded the frictional forces of the sleeves' thumbscrews, causing the sample to slip out of the tester before the bond could experience failure. To counteract this, the two thumbscrews in the middle of the upper and lower sleeves were replaced by 8-32 socket head cap screws, which could be tightened by an Allen wrench. This would ensure that bonded samples were secured to the tester throughout the duration of strength evaluation. Changes to the experimental procedure and test results confirming that these adjustments would not affect the measured values are discussed later in this chapter.

4.2 Sample Preparation

4.2.1 Adhesive Preparation

Sample adhesives of polymer blends were created following Olivia Boyd's method of preparation,²² which itself had been adapted from Koob's original procedure.⁴ Seven different acrylic polymer adhesives were created and subsequently investigated for their tensile fracture strength in this study. The different polymer blends were cast from 50 wt% solutions purely in acetone, such as to mimic art conservation practices, and are labeled by the ratios of their B-72 to B-48N content. In this thesis 1:0, 7:1, 3:1, 1:1, 1:3, 1:7, and 0:1 B-72:B-48N adhesive samples were created and subsequently applied to glass rod samples to be tested for their tensile fracture



Figure 4.2: Photograph of the CATS Tester along with all of the available masses used for stress-testing. A glass rod sample has been secured to the upper and lower sleeves of the tester.

strength.

For each of the polymer blends, an initial 1 g solution was created by weighing out and mixing 2 parts acetone to 1 part polymer resin. After sealing this solution and allowing it to settle for 1-2 hours at room temperature, the contents dissolved into a homogenous mixture. The solution container was then weighed before being set open under the fume hood, where 50 wt% of the acetone was evaporated. In order to create consistent sample adhesives, the solution containers were weighed after solvent evaporation to ensure that an exact 1:1 solvent:polymer solution remained, at which point the adhesive was ready to apply. If too much evaporation had occurred, a correctional amount of acetone was added to the solution prior to its application to the testing samples.

4.2.2 Glass Rod Sample Preparation

The CATS tester was designed to evaluate the tensile fracture strength of polymer adhesives when cured as bonds between two identical segments of borosilicate glass rod adherents. In order to prepare glass rods for adhering, 24-inch long, 6 mm diameter glass rods purchased from McMaster-Carr were broken into 2-inch segments using a Scientific Glass Tubing Cutter. Prior to breaking apart the rods, a line was marked along the length of the segments with a permanent



Figure 4.3: Photograph of drying rack used to adhere and dry glass rod samples. Thumb screws at the top of the chamber are used to clamp together ends of the glass rods. The chamber includes circular indentations to encourage airflow during solvent evaporation.

marker in order to reproduce the original axial alignment when the rods were reattached during bond application.

Once the rods had been scored, marked, and broken into segments, their ends were wiped using Kimwipes and acetone. This was done to ensure that the rods were degreased and therefore provided a clean interfacial surface for an adhesive line to be applied.

To apply the bond, half of the glass rods were first loaded horizontally onto the bottom portion of the drying rack's sample channel, pictured in Figure 4.3. Adhesive was applied to the ends of the remaining rods using a Size 0 Blick Economy Golden Taklon flat brush. Once the adhesive had been applied to the end of a glass rod segment, the segment was placed at the upper half of the drying rack's sample channel. The segment was then pushed by using the drying rack's thumb screws to make contact with the segment previously placed at the bottom half of the channel. It was discovered during the MET's reconstruction of Tullio's Adam that an optimal pressure of 100 psi was required for the 3:1 B-72:B-48N adhesive to attain maximum adhesion during drying.⁵ As such, the thumb screws on the drying rack were tightened just enough to assert 'finger-strength' pressure to the glass rod samples as this corresponded to approximately 100 psi when considering the geometry of our 6 mm diameter glass rods.²²

It was crucial to apply an even but thin line of adhesive to the join of the rods. Firstly, a

thinner bond line ensured that we were measuring the adhesive strength, or the interfacial strength between the adhesive and the substrate, which is a better indicator as to how a bond may withstand a conserved object's load than the adhesive's cohesive strength.³ Furthermore, because this study has direct applications to the field of art conservation, it was necessary to emulate the standard practices of a conservator, who may avoid thicker bond lines in order to minimize the amount of displacement that occurs when re-attaching fragments of an object back together. The application of a thin yet continuous bond line during sample preparation was confirmed by the secretion of small adhesive bubbles along the exterior of the join as the rods were clamped together. These bubbles were mechanically removed by hand prior to CATS testing once the bond had fully dried.

After the glass rods had been adhered and clamped together on the drying rack, the drying rack was left upright in the fume hood for 72 hours. The vertical position of the drying rack prevented the adhesive in the join from pooling over to one side and also allowed gravity to work together with the adhesive strength to bond the glass rods together.⁸ As the drying rack design includes circular holes in the middle of each sample channel slot, sufficient airflow around the bond line was provided during the 72 hours of drying to facilitate solvent evaporation evenly around the join's perimeter

4.3 Experimental Procedure

4.3.1 Measurement Procedure: Improvements over Previous Method

Following 3 days of drying, the adhesive bubbles were gently removed from the exterior of the join prior to CATS testing. Glass rod samples were first inserted into the lower sleeve of the tester and then attached to the upper sleeve. Once the sample was tightly secured to the tester, the hanger was attached to the lower sleeve such that slotted weights may be added to stress-test the bond. The weights available for CATS testing included ten 10 g masses, twenty-five 20 g masses, four 50 g masses, two 200 g masses, and nine 500 g masses.

For the first sample in a batch of 6 rods, large weights were freely added until the bond was broken—giving an approximate estimate of the adhesive's tensile fracture strength. For the

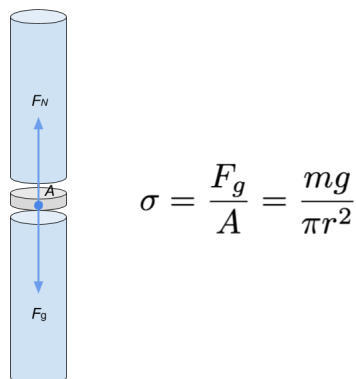


Figure 4.4: Forces acting on a glass rod sample during CATS testing. Tensile fracture strength is calculated by dividing the gravitational force at the weight of failure by the cross-sectional area of the glass rods.

remaining 5 rods, 75% of the weight at failure for the first rod was immediately added to the hanger before 20 g of weight were added every 5 seconds. While Olivia's experimental procedure originally involved adding 50% of the initial weight at failure rather than 75%, preliminary testing that followed Olivia's procedure showed that for the polymer blends much stronger than B-72, 20 g masses would often fill up the hanger before bond failure would occur. As such, 20 g masses would have to be removed and replaced with larger masses before proceeding to add more 20 g weights every 5 seconds. As this would cause jostling to the hanger and potentially introduce non-tensile forces to the bond under evaluation, we chose to immediately add 75% of the first rod's weight at failure to reduce the need to remove and replace weights throughout testing.

For each of the rods, the weight at failure was recorded and subsequently converted to measures of tensile fracture strength, using equation 2.1. As 6 mm diameter rods were used, the cross-sectional area of the bond used to calculate tensile fracture strength was 28.3 mm². The tensile fracture strengths of six glass rod measurements were averaged to provide one data point for each polymer adhesive under evaluation. Because some glass rod samples would fail during the drying process prior to any CATS testing, some trials include an average of five glass rods rather than six.

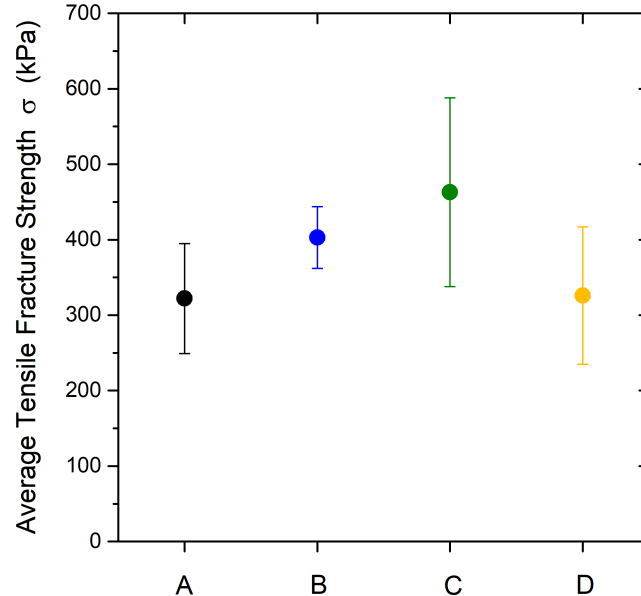


Figure 4.5: The recorded tensile fracture strength of B-72 adhesive bonds measured on the CATS tester: Olivia Boyd’s reported measurement (A) is shown in black, the measurement following Boyd’s testing procedure (B) is shown in blue, the trial using the new testing procedure and thumb screws (C) in green, and the trial using the new testing procedure and socket head cap screws (D) in yellow. Each measurement falls within one standard deviation away from another.

4.3.2 Preliminary Testing and Comparison with Previous Results

In order to confirm that changing the CATS testing procedure by increasing the initial weight added to the rods would not impact the measured weight at failure, some preliminary testing intended to reproduce Olivia’s measurement of B-72 tensile fracture strength was conducted for comparison.

The CATS tester was used to perform three preliminary evaluations, shown in Figure 4.5, of B-72’s tensile fracture strength while: (1) using the thumb screws and Boyd’s original procedure, (2) using the thumb screws and the newly proposed procedure, and (3) using 8-32 socket head cap screws and the new procedure. In following Boyd’s original procedure, the average tensile fracture strength of B-72 was determined as 322 ± 73 kPa, in comparison to Boyd’s measurement of 403 ± 41 kPa. The updated experimental procedure yielded an average strength of 463 ± 125

kPa and the updated procedure with the replacement of thumb screws for socket head cap screws yielded an average of 326 ± 91 kPa. As results of the measured B-72 tensile strengths under each of these conditions fell within one standard deviation of another, the results conveyed confidence that adjustments to the CATS tester design and experimental protocol did not cause a meaningful impact on the recorded measurements. Therefore, the methodology for quantifying the adhesive strength of B-72:B-48N polymer blends was fully developed.

CHAPTER 5

RESULTS AND DISCUSSION

5.1 Evaluations of Tensile Strength: Results of CATS Testing

5.1.1 Reproducibility of B-72 and B-48N Tensile Strength

Prior to evaluating the tensile fracture strengths of adhesives formed out of B-72:B-48N blends, the CATS tester was used to evaluate the tensile fracture strength of neat B-72 and neat B-48N adhesives. For both the neat B-72 and B-48N adhesives, three trials, each using six adhered glass rod samples, were run on the CATS tester. Figure 5.1 provides the results of tensile fracture strength for both the B-72 and B-48N adhesives for each trial. For each polymer, trial measurements were all within one standard deviation from one another and thus demonstrated good reproducibility.

The average tensile fracture strength of polymers in this thesis is reported as the average strength measured across trials, where each trial itself represents an average of six measurements. The propagated error across multiple trials was determined using the formula,

$$\sigma_{avg} = \sqrt{\frac{\sum_{i=1}^N \sigma_i^2}{N}}, \quad (5.1)$$

where σ_i denotes the standard deviation of each trial and N represents the number of trials conducted.

As such, we determined the average tensile fracture strength of B-72 as 440 ± 99 kPa and the average tensile fracture strength of B-48N as 874 ± 78 kPa. For a T_g difference of just 10 °C, it appeared that B-48N had twice as much tensile fracture strength than B-72. From these initial results, it was expected that the average tensile fracture strength for each of the polymer blends would fall between the range of 440 and 874 kPa, with higher concentrations of B-48N leading to higher measures of tensile fracture strength in the blends.

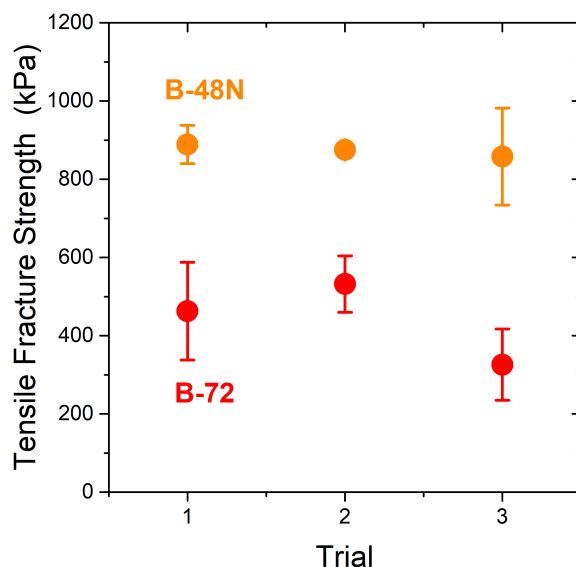


Figure 5.1: Tensile fracture strength of neat B-72 and B-48N adhesives for three different trials run on the CATS tester. Error bars are given as the standard deviation of tensile strength for a set of six rods. The average tensile fracture strength of the B-72 (in red) is 440 ± 99 kPa and 874 ± 78 kPa for the B-48N (in orange).

5.1.2 Tensile Strength of B-72:B-48N Blends

For each of the remaining polymer blends under investigation, two different trials of CATS testing were conducted to measure tensile fracture strength. In that there was much variability in the strength results of the 1:3 B-72:B-48N blend, a third trial of CATS testing was conducted for this particular blend. Figure 5.2 provides a plot of the measured tensile fracture strength against the percentage of B-48N present in the adhesive blend. A table with each blend's measured average tensile fracture strength is provided in Table 5.1

In analyzing Figure 5.2, we observe that tensile fracture strength generally increases with increasing B-48N content as expected. However, in observing the difference in tensile fracture strength between neat B-72 and the 7:1 B-72:B-48N blend, we can notice how even the small addition of B-48N in the adhesive system leads to a dramatic increase in tensile strength. While the neat B-72 adhesive has an average tensile strength of 440 ± 99 kPa, the 7:1 B-72:B-48N blend, which consists of 12.5% B-48N, exhibits an average tensile fracture strength of 628 ± 145 kPa.

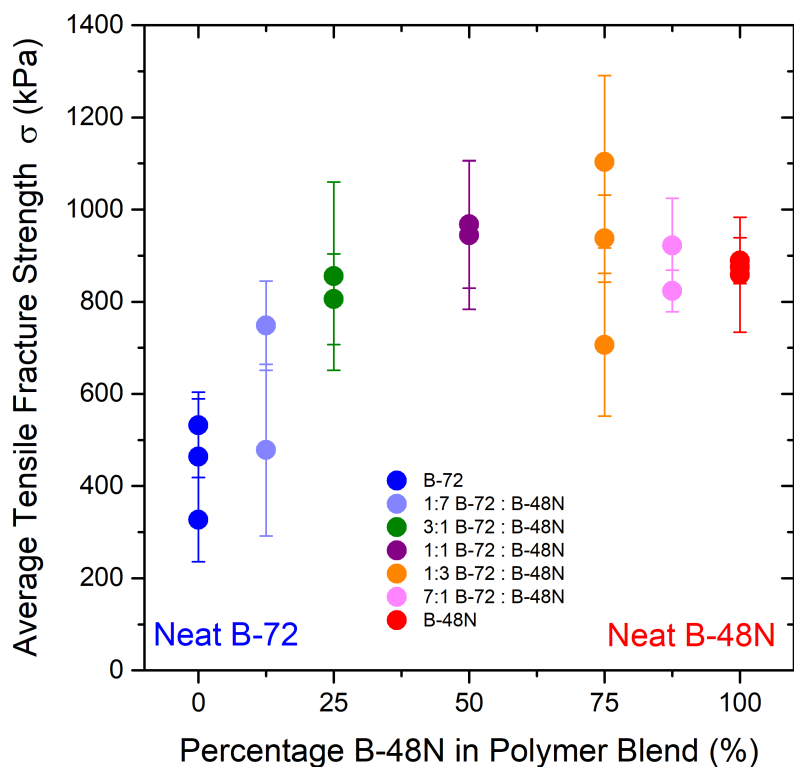


Figure 5.2: Average tensile fracture strength of all blends measured in this thesis plotted against the percentage B-48N present in the blend. Each data point in this plot represents a trial, which averaged the recorded tensile fracture strengths of six adhesive samples. Error bars were determined by each trial's standard deviation.

Polymer Blend	Percentage B-48N in Blend (%)	Average Tensile Fracture Strength σ (kPa)
B-72	0	440 ± 99
7:1 B-72:B-48N	12.5	628 ± 145
3:1 B-72:B-48N	25	830 ± 160
1:1 B-72:B-48N	50	956 ± 150
1:3 B-72:B-48N	75	915 ± 150
1:7 B-72:B-48N	87.5	872 ± 145
B-48N	100	874 ± 78

Table 5.1: The average tensile fracture strength σ for all polymers investigated in this study. Each measurement is determined as the average strength across trials and uncertainty is determined by error propagation discussed above.

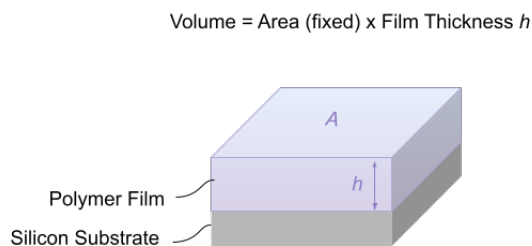


Figure 5.3: Sample geometry of a polymer thin film. The polymer film is spin-coated onto a square silicon substrate of fixed area. As such, changes in the polymer's volume correspond to changes in its film thickness h .

Interestingly though, with only 50% B-48N content, the B-72:B-48N blend exhibits the same tensile fracture strength as pure B-48N. This implies that the addition of B-48N increases the tensile fracture strength of cured adhesive bonds only up to a certain loading level.

5.2 Evaluations of Glass Transition: Results from Ellipsometry

5.2.1 A-11 Control: PMMA

In order to ensure that ellipsometry measurements taken for this thesis would be precise and accurate, two sample films of a well-understood polymer in our lab, A-11 (PMMA), were measured under ellipsometry and analyzed for its glass transition prior to any measurement of the B-72 and B-48N blends. In this subsection, the results of A-11 measurements are used to lend confidence in the experimental procedure, as well as illustrate the methods of data analysis used to extract T_g and determine plots of thermal expansivity α for all polymer samples studied under this thesis.

In Chapter 2, we noted that we may observe the glass transition by looking at a plot of a polymer's volume versus temperature and identifying two different linear slopes corresponding to that polymer's glassy or rubbery state. In that polymers prepared for ellipsometry are spin-coated onto square silicon substrates of fixed area, changes in a polymer's film thickness h against temperature correspond to changes in its total volume with temperature. This may be more clearly understood through the illustration of the film sample geometry provided in Figure 5.3. Therefore,

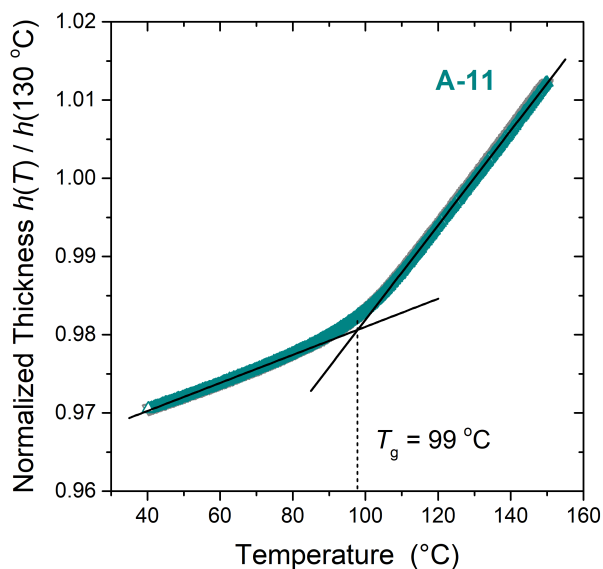


Figure 5.4: Normalized film thickness versus temperature for two A-11 samples. The dark blue data overlays the grey data, indicating excellent agreement between the two different samples. Lines of best fit are superimposed on the low and high temperature regions and T_g is measured as the intersection at 99 ± 2 °C.

by designating film thickness as a proxy for measuring a polymer's volume, we utilized the film thickness versus temperature plots generated from the ellipsometry data to observe that polymer's glass transition.

Figure 5.4 provides a plot of the experimentally measured A-11 film thickness versus temperature for two different samples, where each sample has been normalized by its film thickness at 130 °C for comparison purposes. Each sample was prepared and measured using the protocol detailed in Chapter 3. The two films were between 790 and 830 nm in thickness after annealing, and show great agreement with one another.

As expected, we observe that the linear slopes of film thickness versus temperature differ in the high and low temperature regions of the plot and correspond to the rubbery and glassy states of the polymer, respectively. To determine the experimental value of T_g from plots of film thickness versus temperature, best fit linear regressions were made to the data in the rubbery and glassy regions and the point of intersection between the two lines was determined as T_g . We determined

the T_g of the two A-11 sample films as 98 °C and 101 °C to give an average T_g of 99 ± 2 °C. As this measured T_g value falls within one standard deviation away from the reported T_g of A-11,¹ we felt confident in proceeding with ellipsometry measurements of the remaining polymers.

In that the glass transition does not occur instantaneously at T_g but rather over a range of temperatures, we may more closely observe the glass transition for its shape and breadth by taking a numerical derivative of the $h(T)$ data and observing changes in the polymer's thermal expansivity over temperature. Significant effort was devoted to developing a method that calculates the polymer's thermal expansivity from the experimentally obtained film thickness data:

Initially, thermal expansivity was calculated by taking the numerical derivative,

$$\alpha = \frac{h(T + \frac{\Delta T}{2}) - h(T - \frac{\Delta T}{2})}{h(130^\circ\text{C}) * \Delta T}, \quad (5.2)$$

where $\Delta T = 4.2$ °C was determined to produce good values of α based on a previous study conducted by Kawana and Jones.²³ After taking the derivative, the locally weighted scatterplot smoothing (LOWESS) method provided in the OriginLabs data processing software was used to reduce noise in the data. The LOWESS method, which uses the weighted regression function

$$w_i(x) = (1 - (\frac{|x-x_i|}{d_i})^3)^3$$

with x_i as the point being smoothed and $2d_i$ as the smoothing range of the data, was used to fit the data surrounding each data point to a linear function and place more importance on the data points closest to the point being smoothed.⁹ Although this was the described method of extracting thermal expansivity from experimentally gathered film thickness data in Benjamin Kasavan's Honors thesis⁹, we found that this method would over-emphasize oscillatory noise in the liquid plateau of the plot.

As such, to determine the thermal expansivity α , a new method in which the slope of a linear regression through the film thickness data points in a specified bin size was utilized. Bin sizes corresponding to a ΔT of 4.2, 7, and 10 °C were tested and it was found that fitting the slope of the film thickness in a 10 °C range best smoothed the oscillatory noise without losing any non-

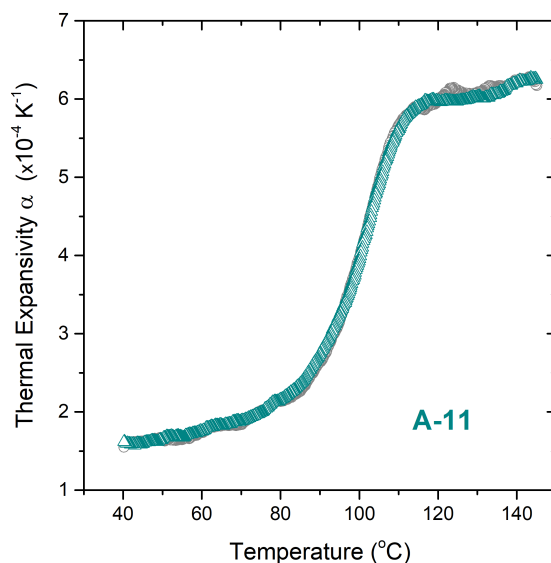


Figure 5.5: Thermal expansivity α as a function of temperature for two A-11 samples. The curve between the two plateaus represents the glass transition of the polymer from a liquid to solid on cooling.

linear aspects of the plot. Therefore, slopes of linear regression lines through the film thickness data points in a range of 10 °C were first calculated and then normalized by $h(25\text{ °C})$, the average film thickness of the sample from between 23 – 27 °C. Figure 5.5 provides a plot of the thermal expansivity α of A-11 versus temperature determined from this method. From this plot, we can clearly observe that A-11 is in its liquid state above 110°C, transitioning from between 110 to 80 °C, and locking into its glassy state from below around 80°C.

5.2.2 Pure B-72 and B-48N

To begin our study into polymer blend glass transitions, three film samples of neat B-72 with thicknesses of 804, 830, and 844 nm and three film samples of neat B-48N with thicknesses of 820, 875, and 885 nm were each evaluated using the ellipsometer.

Figure 5.6(left) provides a plot of the experimentally gathered film thickness versus temperature for three samples of B-72, where each sample has been normalized by its average thickness over 23 – 27 °C for comparison. For each sample, linear fits of the glassy and rubbery region

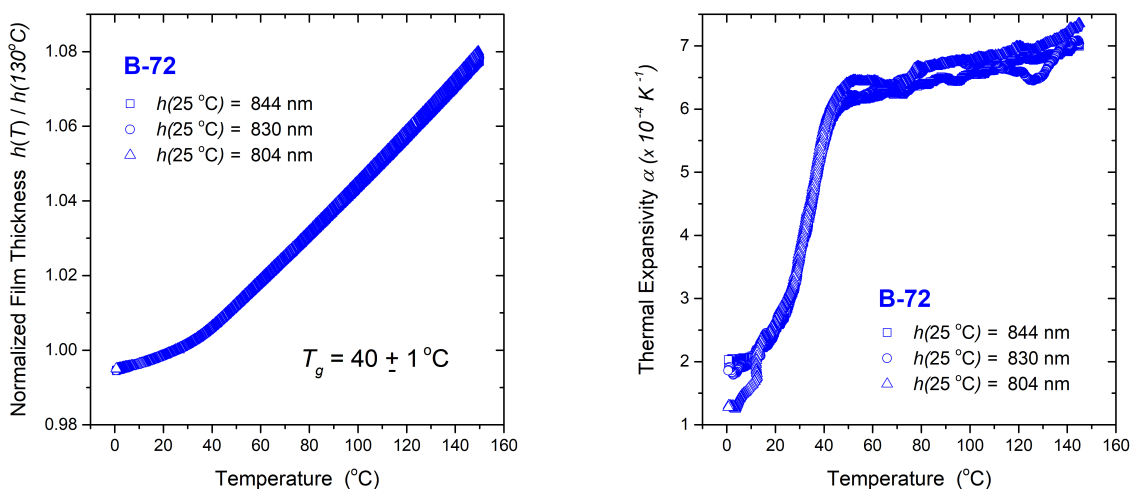


Figure 5.6: (Left) Normalized film thickness versus temperature for three samples of B-72. The average T_g for this set of samples was found to be 40 ± 1 °C. (Right) Thermal expansivity versus temperature for three samples of B-72.

were used to identify T_g . For the three samples measured, T_g was determined as 39, 41, and 39 °C to give an average T_g value of B-72 as 40 ± 1 °C, which is in good agreement with the literature value.¹

In Figure 5.6(right), we can visualize the range of the glass transition of B-72 through its thermal expansivity versus temperature graph. On cooling, there is a sharp decrease in the thermal expansivity, indicating that the glass transition rapidly begins at around 45 °C before stopping at around 20 °C. Comparing the data in Figure 5.6 together, we can determine that at room temperature, B-72 has just about finished transitioning into its solid state, which explains why it is able to more cooperatively adjust to stresses imposed by a conservation object than polymers such as A-11 that have long finished their glass transition at room temperature.

Figure 5.7(left) provides a plot of normalized film thickness for the three different samples of B-48N versus temperature. The T_g of each sample was measured as 50, 49, and 51 °C, respectively, to give an average T_g of 50 ± 1 °C. As such, we find that the T_g of B-48N is 10 °C higher than the T_g of B-72, in agreement with the reported literature values.¹ In observing the shape of the glass transition through Figure 5.7(right), we can observe that B-48N has a much wider breadth of

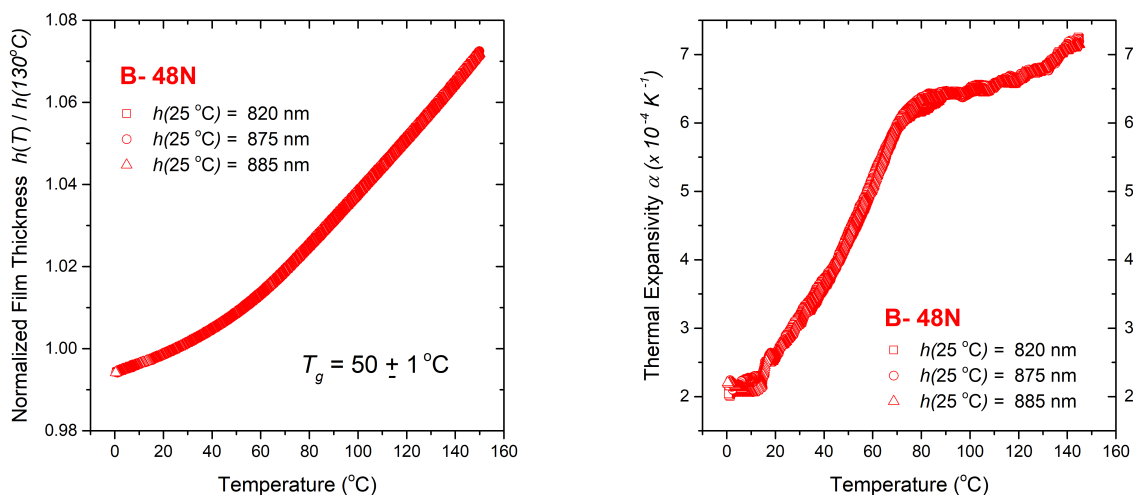


Figure 5.7: (Left) Normalized film thickness versus temperature for three samples of B-48N. The average T_g was measured as $50 \pm 1^\circ\text{C}$. (Right) Thermal expansivity versus temperature for three samples of B-48N.

transition than B-72, spanning from $80 - 20^\circ\text{C}$. The broader glass transition of B-48N compared to the sharp and narrow glass transition of B-72 may imply that B-48N is less sensitive to temperature changes and more capable of supporting stresses for a wider range of temperatures than B-72, which may be important in the context of storing, displaying, or transporting conservation treatments in hotter temperatures than in a climate-controlled museum.

5.2.3 Blends of B-72 and B-48N

For each of the remaining polymer blends under investigation, three sample films of thicknesses between 720 and 960 nm were measured with the ellipsometer and analyzed for the glass transition on cooling. Figure 5.8 provides results of each polymer blend's glass transition temperature T_g and thermal expansivity α in order of increasing B-48N percentage in the blend.

We notice from the plots of normalized film thickness versus temperature that the temperature at which the polymer blends fall out of equilibrium on cooling increases as the B-48N content increases. We find that the addition of B-48N to a polymer blend therefore raises the overall T_g of a B-72:B-48N blend values that generally agree with the Fox equation (Eq. 2.3) predictions.

A table of all the measured T_g values in comparison to the reported or predicted T_g values for all polymers studied in this thesis is provided in Table 5.2.

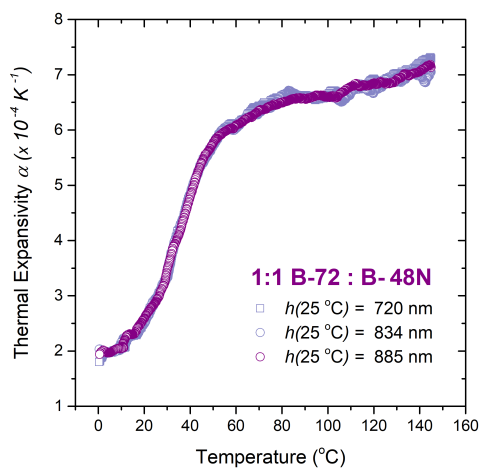
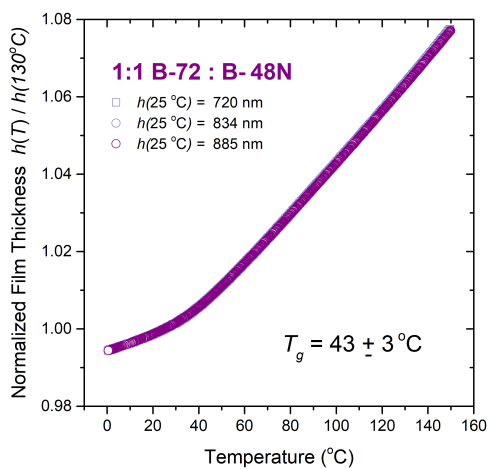
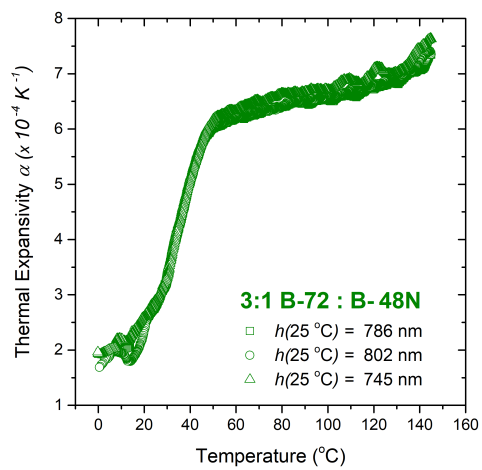
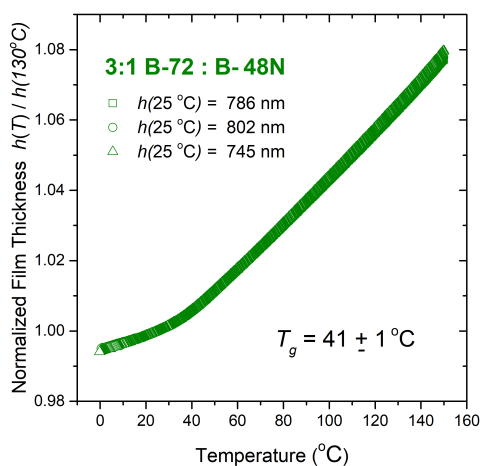
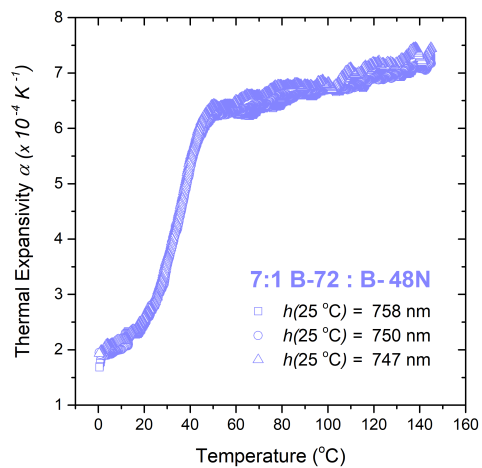
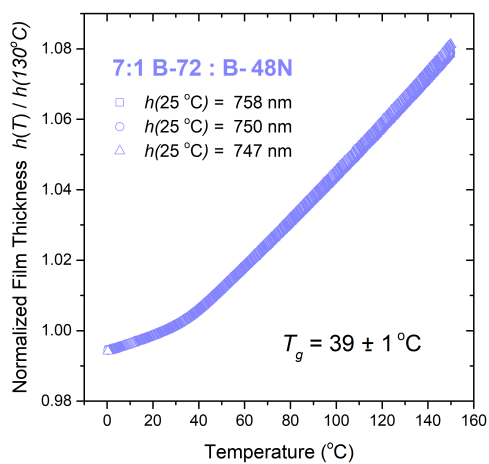
Table 5.2: The reported T_g values from Ref. [1] of all polymers investigated in this study and the experimental values of T_g gathered for this thesis. Estimated T_g values have been calculated from the Fox equation.

Polymer(s)	Reported or <i>Estimated</i> T_g ($^{\circ}\text{C}$)	Measured T_g ($^{\circ}\text{C}$)
A-11	100	99 ± 1
B-72	40	40 ± 1
7:1 B-72:B-48N	41	39 ± 1
3:1 B-72:B-48N	42	41 ± 1
1:1 B-72:B-48N	44	43 ± 3
1:3 B-72:B-48N	47	47 ± 1
1:7 B-72:B-48N	48	49.1 ± 1
B-48N	50	50 ± 1

Additionally, we notice from the plots of thermal expansivity versus temperature shown in Figure 5.8 that the shape of a polymer blend's glass transition most closely resembles the glass transition shape of whichever resin was in greater concentration in the blend. In particular, the breadth of temperatures over which the glass transition occurs increases with increasing proportions of B-48N found in the blend. Since the glass transition of B-48N occurs over a wider range of temperatures than that of B-72, we might expect polymer blends with a glass transition shape resembling that of B-48N to have greater stability and resistance to changes in ambient temperature. This is because the glass transition does not occur so abruptly for these blends as it does in pure B-72. Therefore we can expect polymer blends with larger B-48N content to retain the mechanical properties desired at room temperature for a wider range of temperatures.

Figure 5.9 provides a plot that allows for a greater comparison of each of the polymer blends' glass transition. Here, we observe that all blends with a B-48N content less than 50% have a glass transition shape similar to that of pure B-72. At a 50% concentration of B-48N, we find that the blend takes an intermediate T_g value between that of pure B-72 and B-48N while still taking advantage of the short breadth of B-72's transition. Above a 50% loading level of B-48N, the breadth of the glass transition for each blend increased, spanning a wider range of temperatures

with increasing B-48N content.



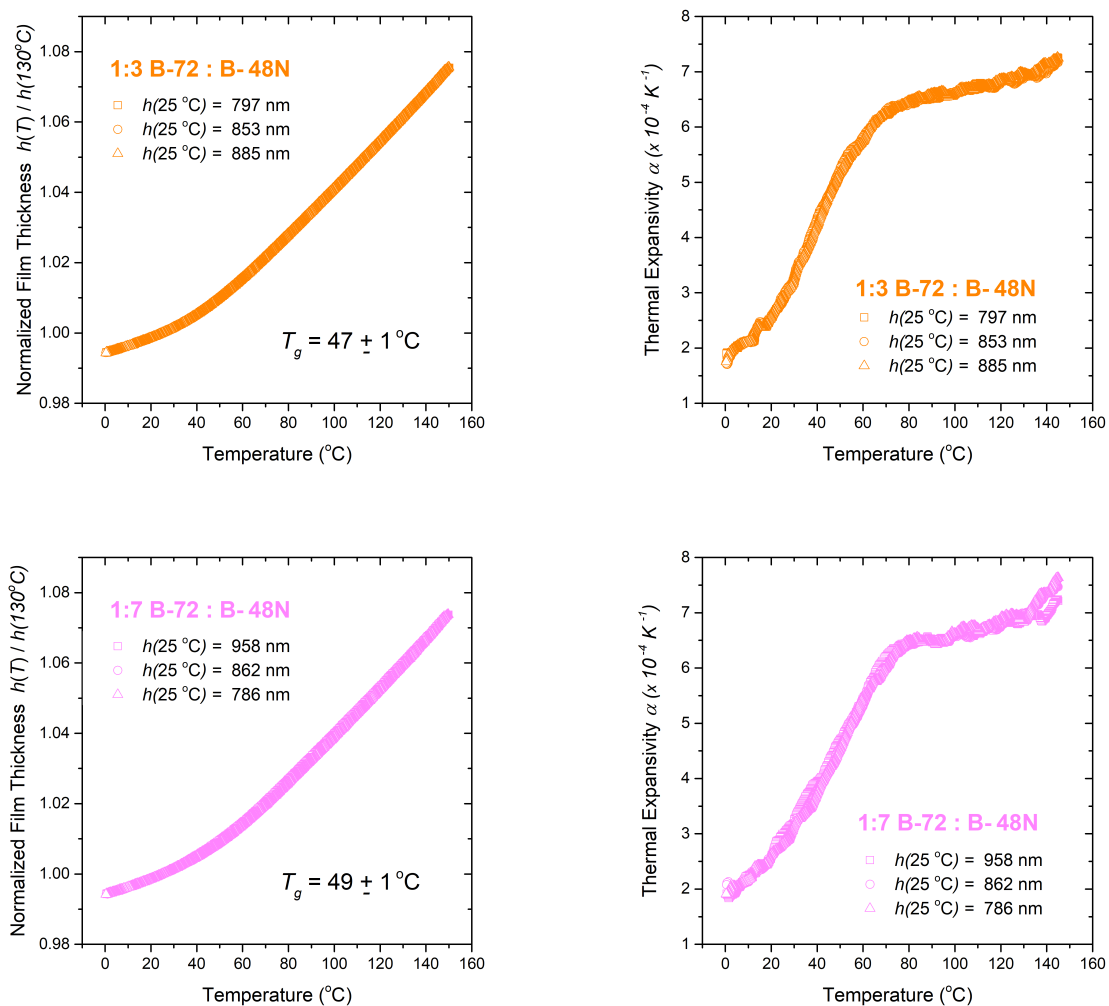


Figure 5.8: Normalized film thickness and thermal expansivity against temperature for all polymer blends studied in this thesis. The plots are presented in the order of increasing B-48N content from top to bottom.

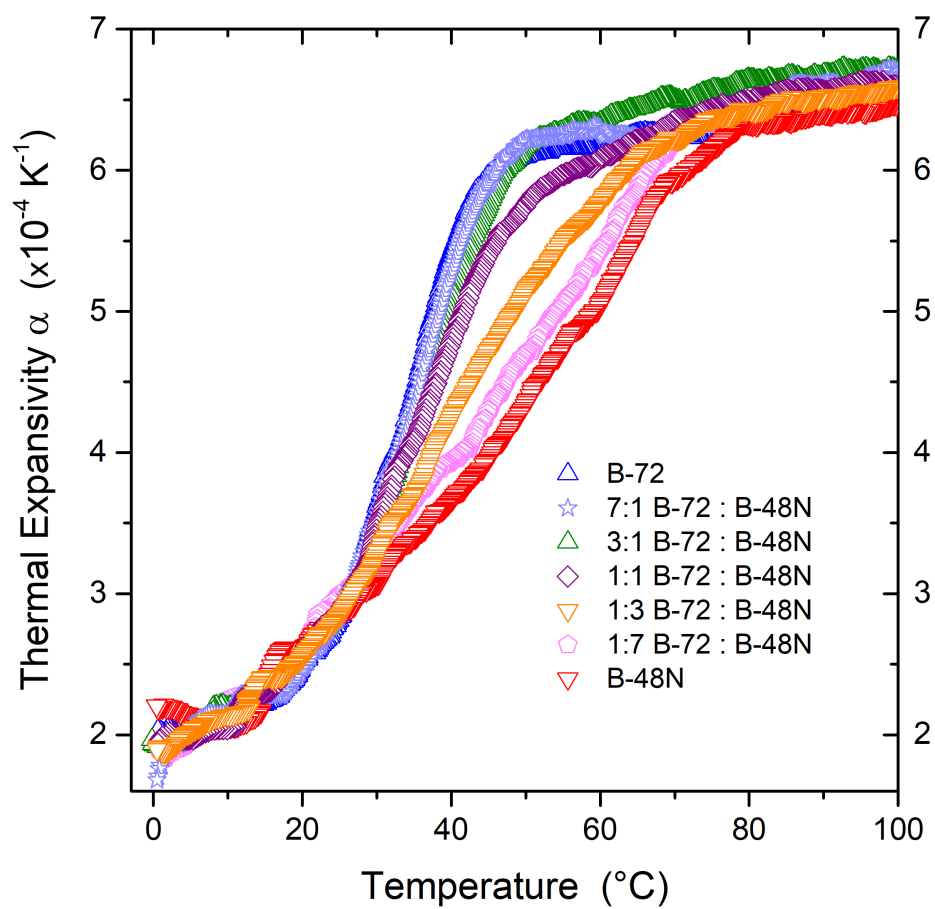


Figure 5.9: Comparison of thermal expansivity versus temperature for all polymer blends under study in this thesis.

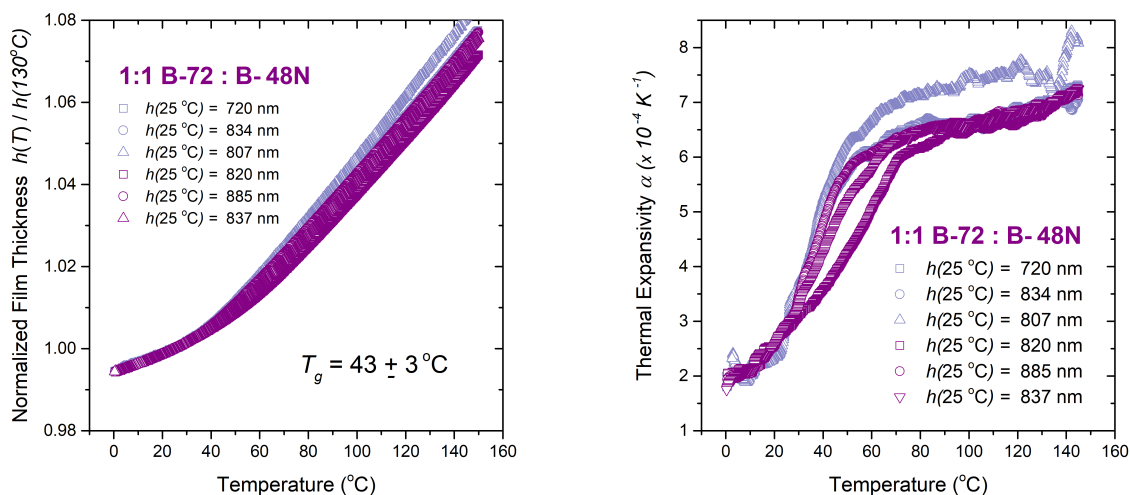


Figure 5.10: (Left) Normalized film thickness versus temperature for six samples of 1-1 B-72:B-48N. (Right) Thermal expansivity versus temperature for six samples of 1-1 B-72:B-48N. The three original film sample measurements are colored in dark purple. The data for the three additional film samples is colored in light purple, with two of these sample measurements showing good agreement with one of the original three sample measurements.

For full disclosure, we mention that there was significant variability in the first three measurements of glass transition for the films of 1:1 B-72:B-48N, as shown in dark purple in Figure 5.10. As such, three additional sample films of 1:1 B-72:B-48N (colored in light purple in the same figure) were measured with ellipsometry. With these new measurements, two of the new measurements agreed very well with one of the initial three measurements. (It is worth noting that the one particularly weird run of the new set measurements was collected in a rush the evening prior this thesis being due to Honors defense committee, which we believe likely accounts for its unusual shape.) Thus, out of the six samples measured, three showed excellent agreement in T_g and shape of glass transition. Therefore, it is these three reproducible measurements that are shown in Figure 5.8. For the comparison plot in Figure 5.9, the thermal expansivity versus temperature curve for one of these reproducible samples was selected. While the reasons behind the variability in data for two of the initial sample films of 1:1 B-72 and B-48N (colored in dark purple) are unknown, it is likely that the different shape and behavior of the last sample film (colored in light purple) is due to rushing of the experimental procedure in order to provide results before the thesis

submission date. Overall, variability in the data suggests that further testing should be conducted for this particular blend.

5.3 Relating Glass Transition to Adhesive Fracture Strength

The data gathered on each polymer blend's glass transition can be used to make qualitative predictions for their use as art conservation structural adhesives. In that the measured T_g values and the shapes of the glass transition for B-72, 7:1 B-72:B-48N, and 3:1 B-72:B-48N do not vary significantly, conservators may find adhesive bonds formed of blends with less than 50% B-48N content to behave similarly to B-72 in terms of stability. Because the glass transition occurs very rapidly for these blends and over a shorter range of temperatures, we may find that each of these blends have a similar, low resistance to elevated temperatures as B-72. Interestingly, although these blends may perform similar to one another in terms of stability, we find that even a small 12.5% addition of B-48N significantly raises the tensile fracture strength of an adhesive bond. As such, conservators should note that a less than 50% addition of B-48N will likely form bonds of similar stability to B-72 but with a much higher strength.

The shapes of the glass transition are distinct from one another for each of the polymer blends with B-48N concentration greater than 50%, with increasing B-48N percentage leading to an increased range of temperatures over which the transition occurs. Despite these differences in breadth of transition however, we find that the average tensile fracture strength of these blends do not vary significantly from another. Therefore, conservators seeking to incorporate a greater than 50% amount of B-48N into a polymer blend should do so with the intent of broadening the adhesive's glass transition and to retain the adhesive's mechanical properties for a wider range of temperatures, rather than for an increase in adhesive tensile fracture strength.

CHAPTER 6

CONCLUSIONS

6.1 Summary of Results

In this thesis, we sought to determine how varying ratios of B-48N incorporated into a B-72:B-48N blend would affect the glass transition and the tensile fracture strength of cured adhesive bonds used for art conservation. Two experimental methods were employed to evaluate the glass transition and tensile fracture strength of seven distinct B-72:B-48N blends:

First, the Conservation Adhesive Tensile-to-Shear (CATS) tester, formerly designed and built by Olivia Boyd²², was used to evaluate the tensile fracture strength of B-72:B-48N blends. Broken glass rod segments were adhered together using the different blends before being subjected to tensile loads and measured for their weight at failure. Initial tests that sought to replicate Boyd's measurements of average B-72 tensile fracture strength found that changing the experimental procedure and CATS tester design did not impact measurements of tensile fracture strength. Prior to evaluating the strength of the blends, tensile fracture strengths of neat B-72 and neat B-48N adhesives were determined as 440 ± 99 and 874 ± 78 kPa respectively. Following stress evaluation of the remaining blends, it was discovered that in general, the average tensile fracture strength of cured adhesive bonds increased with increasing B-48N content in a B-72:B-48N blend. Interestingly, even the small 12.5% addition of B-48N to a blend increased the tensile fracture strength by a significant amount with the 7:1 B-72:B-48N blend exhibiting a strength of 628 ± 205 . However, the strength of the blends did not significantly increase after a 50% loading content of B-48N, and these blends exhibited similar strength to a pure B-48N adhesive.

Next, ellipsometry measurements of each of the blends were conducted in order to track changes in the blend's film thickness and thermal expansivity with temperature. In order to confirm that these measurements would be accurate, two sample films of A-11 (PMMA), a well-studied

polymer in our lab, were first measured. Methods of recording the glass transition temperature, T_g , as well as for extracting the first-order derivative, thermal expansivity α , from the experimentally obtained film thickness versus temperature data were determined. The experimental value of T_g for A-11, 99 ± 2 °C, conveyed confidence in the ellipsometry procedure. Three sample films were spin-coated for each polymer blend and evaluated with ellipsometry to find that the glass transition temperature T_g generally increased with increasing loading levels of B-48N. The measured T_g values of the blends seemed to align well with T_g predictions calculated from the Fox equation.

The glass transition of B-72 was observed to be sharp and narrow, spanning from 45–20 °C, with a measured T_g value of 40 ± 1 °C. Meanwhile, the glass transition of B-48N was much broader, occurring from 80 – 20 °C with a measured T_g value of 50 ± 1 °C. The glass transitions of B-72:B-48N blends resembled the glass transition shape of the polymer resin in greatest concentration, with the 1:1 B-72:B-48N exhibiting both the sharp drop in thermal expansivity and the broader range of transition seen in the glass transitions of B-72 and B-48N respectively.

In comparing plots of tensile fracture strength and thermal expansivity versus temperature for all blends studied in this thesis, we were able to conclude that blends with a B-48N content less than 50% likely exhibit similar stability and low resistance to elevated temperatures as B-72 despite exhibiting a much higher tensile fracture strength than pure B-72. As such, conservators aiming to raise the tensile fracture strength of their treatment adhesives while keeping the performance of the adhesive similar to that of B-72 should incorporate no more than 50% B-48N in their blends. As we increase the B-48N content in the blend past 50%, the tensile fracture strength does not vary much from the strength of pure B-48N, but the shapes of glass transition become increasingly broader and more similar to that of pure B-48N. The broader breadth of glass transition for these blends suggest a greater resistance to creep at elevated temperatures.

6.2 Future Work

Further experiments should be conducted in order to fully understand the mechanical properties of B-72:B-48N blends for use in art conservation. To provide a more comprehensive under-

standing of adhesive blend performance, tensile fracture strength evaluations should be considered under different conditions such as in elevated temperatures, elevated humidity, or following thermal cycling. It is also important to vary the angle at which these blends are stress-tested at in order to illuminate how the blends will perform under a combination of shear, compression, and tensile forces.

Additionally, it is important to note that all ellipsometry measurements taken in this thesis evaluate the glass transition of B-72:B-48N blends under a temperature quench, whereas in art conservation, where the preservation of the object under repair is most heavily prioritized, polymer-based adhesive bonds are cured through a solvent quench. However, as best exemplified by A-11 (PMMA), the structure and stability of a polymer's glassy state are dictated by how that glass was formed. Therefore, the shape and breadth of glass transition may differ depending on whether that polymer was temperature or solvent quenched. As such, the construction of a solvent vapor cell, which may be used in conjunction with the ellipsometer to monitor changes in a polymer's film thickness over solvent evaporation, would provide more accurate understanding of how a polymer-based adhesive bond used in art conservation is formed.

REFERENCES

- (1) Horie, C. V., *Materials for Conservation*, 2nd ed.; Routledge: London, 2013.
- (2) *The Science For Conservators Series: Volume 3: Adhesives and Coatings*; Conservation Unit Museums and Galleries Commission: Routledge, London, 2013.
- (3) Podany, J.; Garland, K. M.; Freeman, W. R.; Rogers, J. Paraloid B-72 as a structural adhesive and as a barrier within structural adhesive bonds: Evaluations of strength and reversibility. *Journal of the American Institute for Conservation* **2001**, *40*, 15–33.
- (4) Koob, S. The Use of Paraloid B-72 as an Adhesive: Its Application for Archaeological Ceramics and Other Materials. *Studies in Conservation* **1986**, *31*, 7–14.
- (5) Riccardelli, C.; Morris, M.; Wheeler, G.; Soultanian, J.; Becker, L.; Street, R. The treatment of Tullio Lombardo's Adam: a new approach to the conservation of monumental marble sculpture. *Metropolitan Museum Journal* **2014**, *49*, 48–116.
- (6) Betz, J. The Influence Of Glass Transition Temperature On The Performance Of Acrylic Thermoplastic Adhesives, Ph.D. Thesis, Columbia University, 2017.
- (7) Russell, R.; Strilisky, B. Keep it together: An evaluation of the tensile strengths of three select adhesives used in fossil preparation. *Collection Forum* **2016**, *30*, 85–95.
- (8) Stein, R. A., *Personal communication*, Nov. 2021.
- (9) Kasavan, B. L. A Study of the Physical Properties of Acrylic Polymers Commonly Used in Art Conservation, Honors Thesis, Emory University, 2019.
- (10) Strahan, D.; Korolnik, S., *Archaeological Conservation*; Universität Tübingen: 2014.
- (11) Alexiou, K.; Müller, N. S.; Karatasios, I.; Kilikoglou, V. The performance of different adhesives for archaeological ceramics under mechanical stress. *Applied Clay Science* **2013**, *82*, 10–15.
- (12) Tan, T.; Rahbar, N.; Buono, A.; Wheeler, G.; Soboyejo, W. Sub-critical crack growth in adhesive/marble interfaces. *Materials Science and Engineering: A* **2011**, *528*, 3697–3704.
- (13) Davis, S. L.; Roberts, C.; Poli, A. Paraloid® B-72/B-48N 1: 1 as an Adhesive for Use in Hot Climates: Literature Review, Laboratory Testing, and Observational Field Study. *Studies in Conservation* **2022**, *67*, 357–365.

- (14) Roth, C. B., *Polymer Glasses*; CRC Press: Boca Raton, 2016; Chapter 1.
- (15) Jones, R. A., *Soft Condensed Matter*; Oxford University Press: 2002.
- (16) Plazek, D. J.; Ngai, K. L. In *Physical Properties of Polymers Handbook*, Mark, J. E., Ed.; AIP Press: 1996; Chapter 12, pp 139 –159.
- (17) Huang, X.; Roth, C. B. Changes in the temperature-dependent specific volume of supported polystyrene films with film thickness. *Journal of Chemical Physics* **2016**, *144*, 234903.
- (18) Hiemenz, P. C.; Lodge, T. P., *Polymer Chemistry*, 2nd ed.; CRC Press: 2007.
- (19) Hecht, E., *Optics*; Pearson Education: 2012.
- (20) Tompkins, H.; Irene, E. A., *Handbook of Ellipsometry*; William Andrew: 2005.
- (21) Fujiwara, H., *Spectroscopic Ellipsometry: Principles and Applications*; John Wiley & Sons: 2007.
- (22) Boyd, O. F. Design and Construction of a Tensile and Shear Strength Testing Apparatus to Study the Addition of Fumed Silica to the Acrylic Adhesive B-72 Used in Art Conservation, Honors Thesis, Emory University, 2020.
- (23) Kawana, S; Jones, R. A. L. Effect of physical ageing in thin glassy polymer films. *European Physical Journal E* **2003**, *10*, 223–230.